TWENTY-THIRD International Conference on composite materials (ICCM23)

Molecular Interactions between Carbon Nanotubes Polyimide Chains Tuned by London Dispersion and Steric Effects

Baode Zhang1,2, Barbara Hecker2 and Günter Reiter2

Snežana D. Zarić3

1 School of Petrochemical Engineer, Liaoning Petrochemical University, Fushun 113001, People's Republic of China, zhangbaode@lnpu.edu.cn

2 Institute of Physics, Albert-Ludwig-University of Freiburg, Hermann-Herder-Str. 3, 79104, Freiburg, Germany.

3 Department of Chemistry, University of Belgrade, Studentski trg 12–16, 11000 Belgrade, Serbia.

The UCC, Belfast Northern Ireland 30th July-4 th August 2023

Outline

- 1 Motivation
- 2 Experimental and methology
- 2.1 In-situ Preparation of nanocompostes of CNT reinforced two Polyimide films
- 2.2 Methodology (computational method)
- 2.3 Characterization
- 3 Results
- 3.1 Experimental results
- 3.2 Calculation results
- 4 Conclusion

1 Motivation London dispersion in Nature

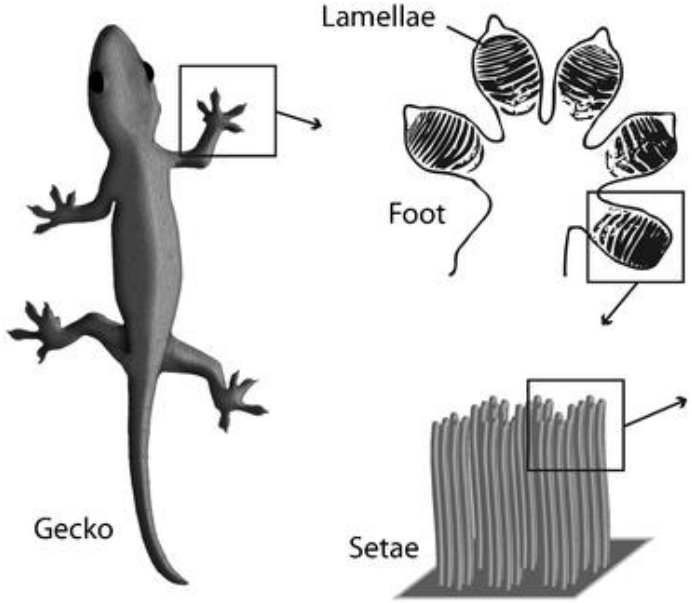

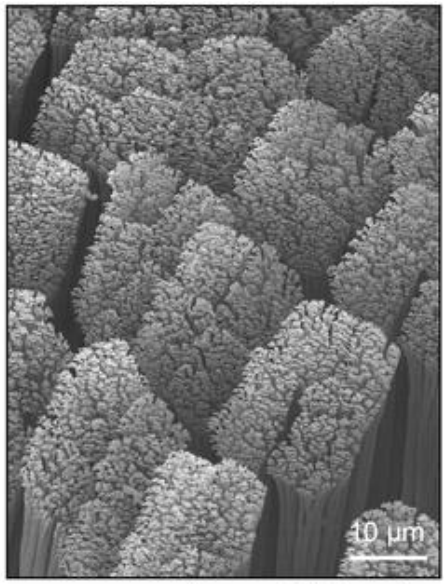

Setae with Spatulae

The ability of geckos – which can hang on a glass surface using only one toe – to climb on sheer surfaces has been attributed to the van der Waals forces, specially London Dispersion Force between these surfaces and the spatulae, or microscopic projections, which cover the hair-like setae found on their footpads

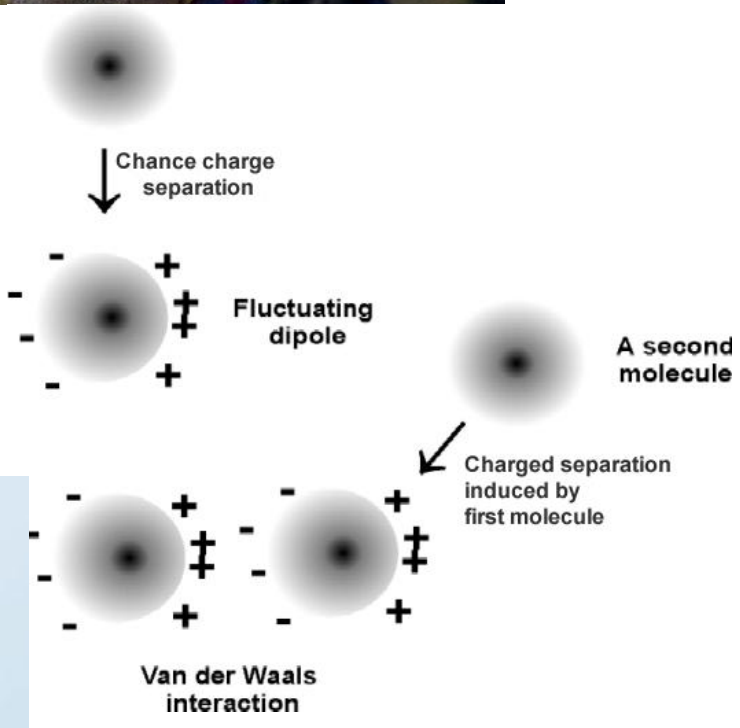

$$E_{\text{disp}} = -\frac{1}{2}\sum_{A,B} C_6^{AB} / r_{AB}^6$$

London dispersion in π electron complex

Pi-Pi interaction

- Strong attractive interactions in π systems have been recognized for several decades. They control such diverse phenomenon, such as

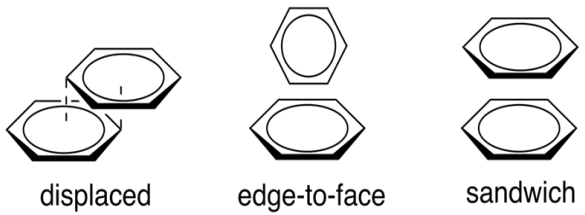

The relative binding energies of these three geometric configurations of the benzene dimer can be explained by a balance of quadrupole/quadrupole and London dispersion forces.

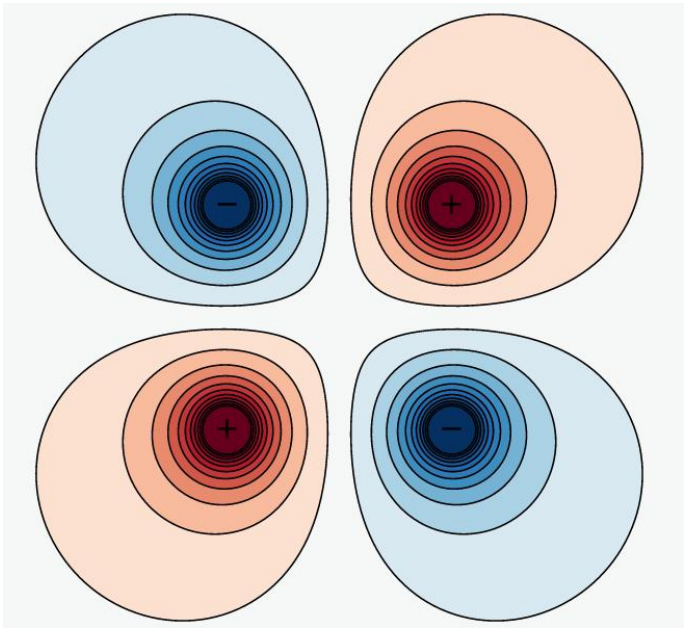

Contour plot of the equipotential surfaces of an electric quadrupole field

Induced dipole forces and London disperson force

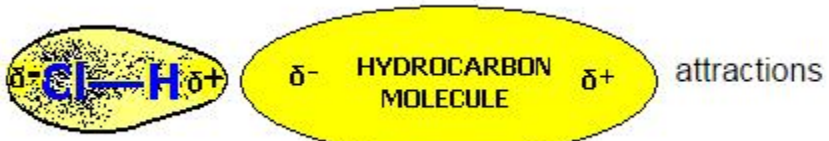

$$\frac{-m_1^2\alpha_2}{16\pi^2\varepsilon_0^2\varepsilon_r^2 r^6} = V$$

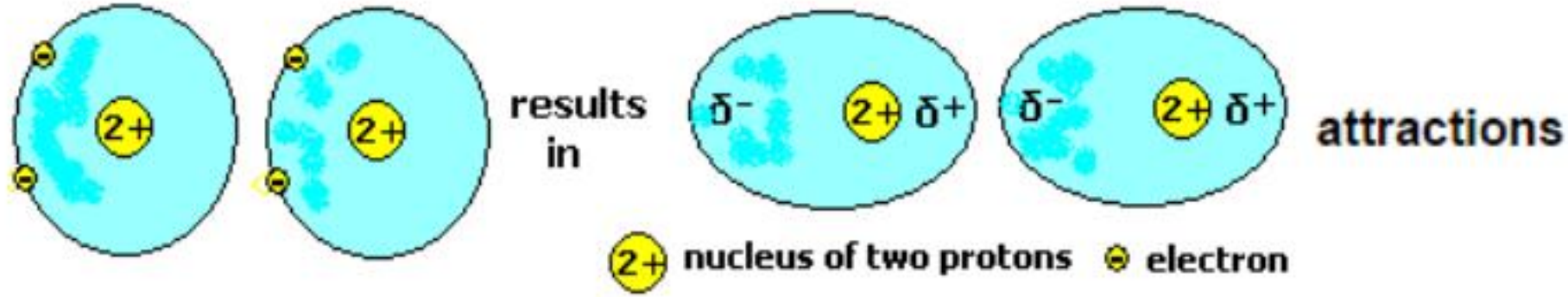

London dispersion dominates the binding energy between two atoms and molecule complexes, chemical reactivity, molecular recognition, self-assembly, nanostructure, heterostructure with delocalized π electrons within nanocomposites as an attractive forces

steric effect

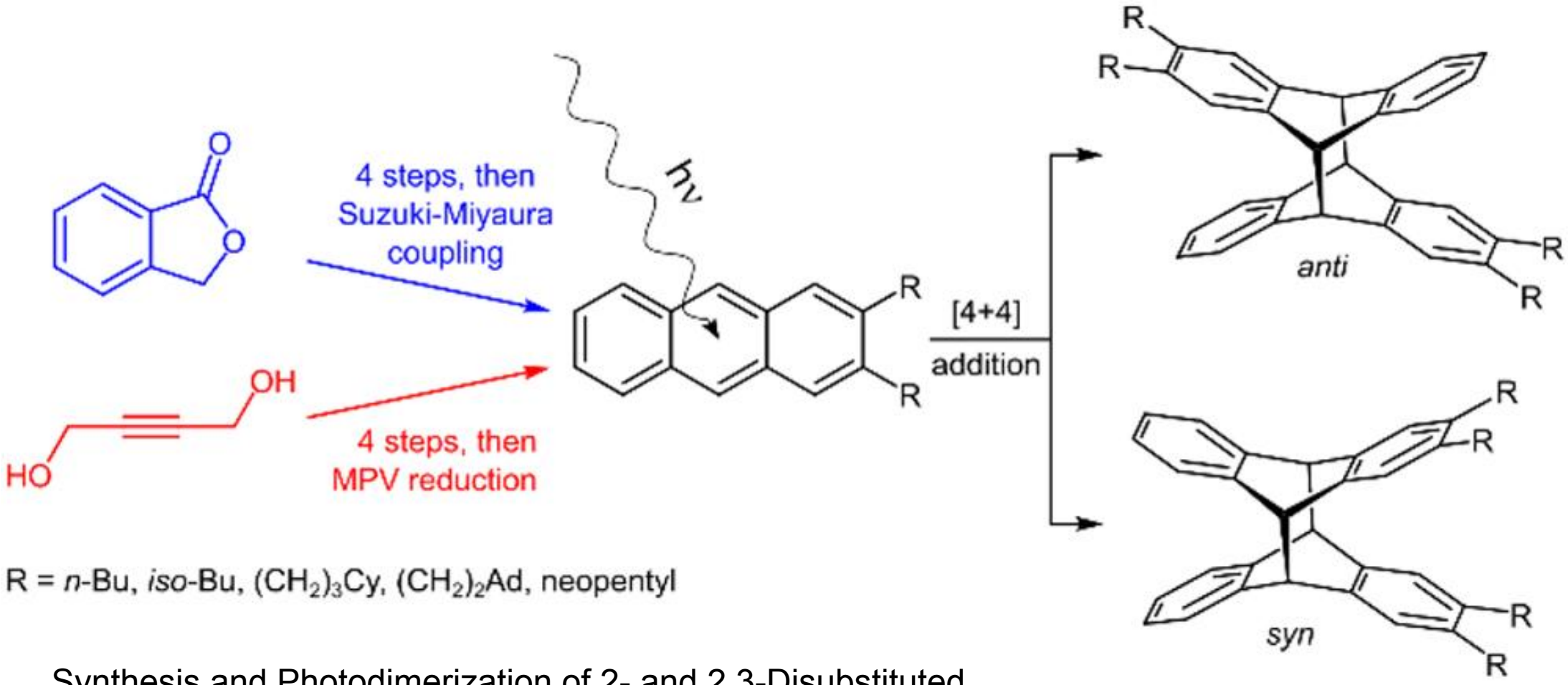

Synthesis and Photodimerization of 2- and 2,3-Disubstituted Anthracenes: Influence of Steric Interactions and London Dispersion on Diastereoselectivity

The balance between London dispersion and Steric hindrance

The interaction energy, stability and conformation, nanostructure of atom and molecule complexes with van der Waals (vdW) bonding are often determined by the interplay between attractive London dispersion forces and repulsive forces due to the Pauli principle.

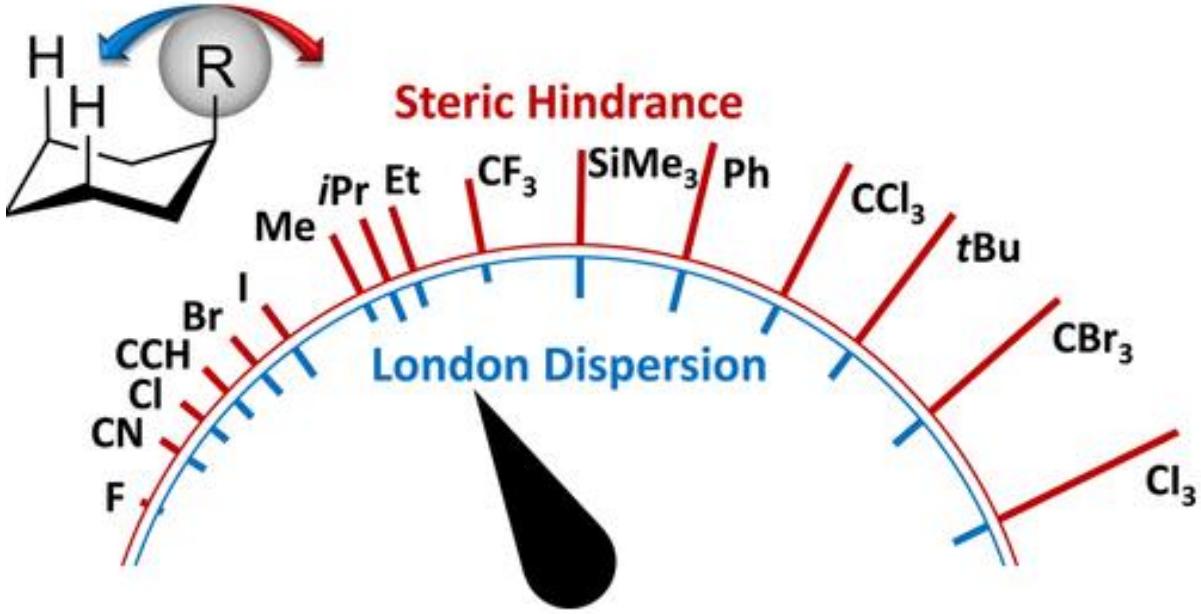

Ref. London Dispersion Helps Refine Steric A- Values: Dispersion Energy Donor Scales

Application of CNT/PI nanocomposites

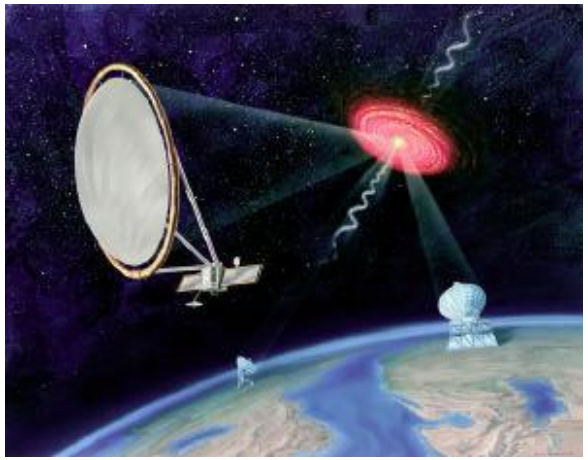

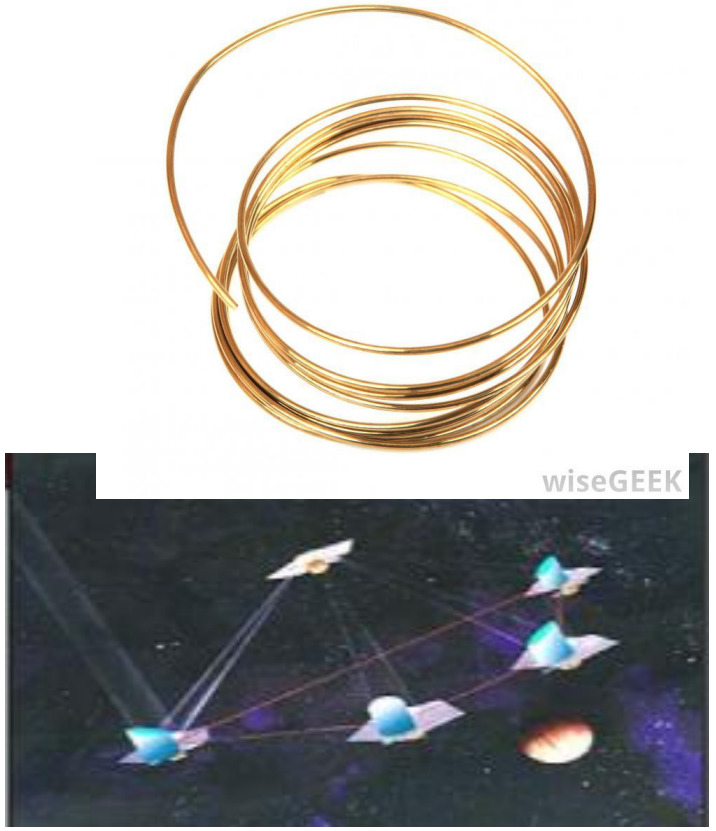

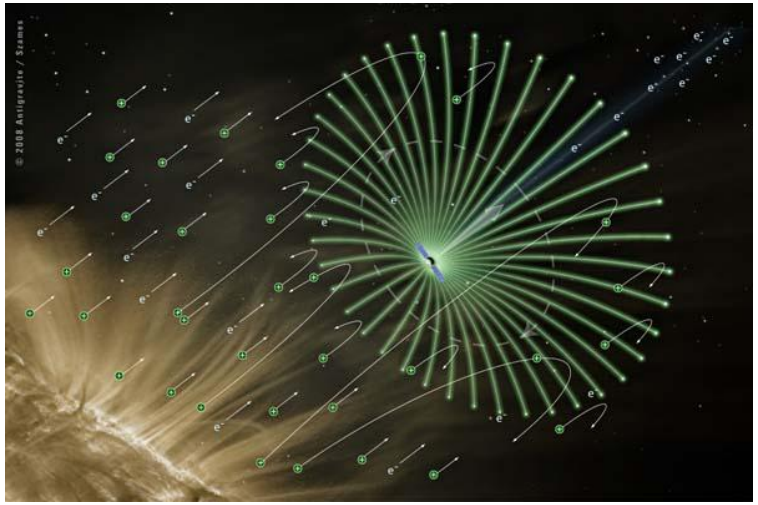

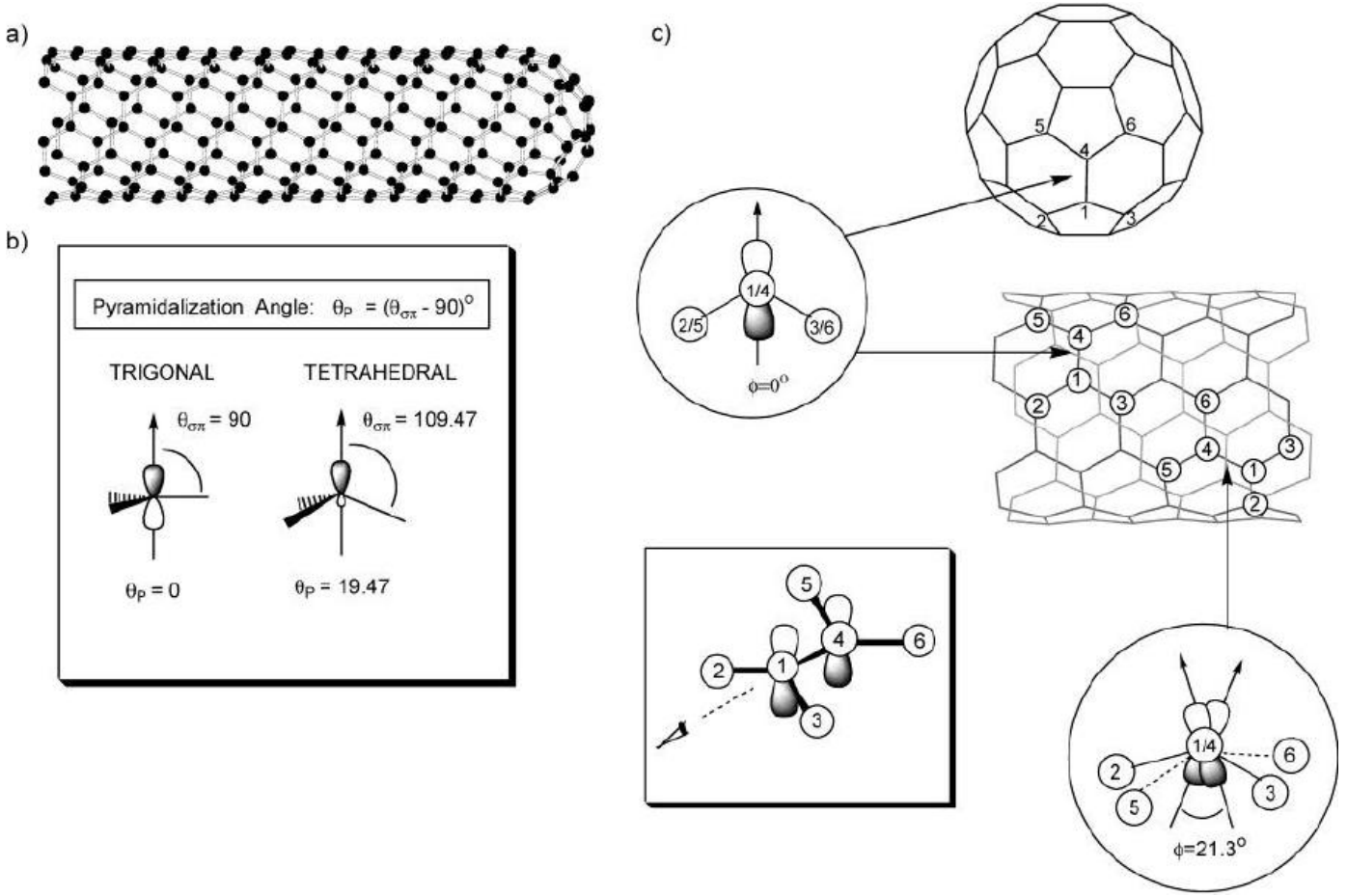

SWNT and its local strain

a) Metallic (5,5) SWNT;
b)Pyramidalization angle (θP);
c)The π-orbital misalignment angles (Φ) along the C1-C4

Advantage of CNT/PI nanocomposites

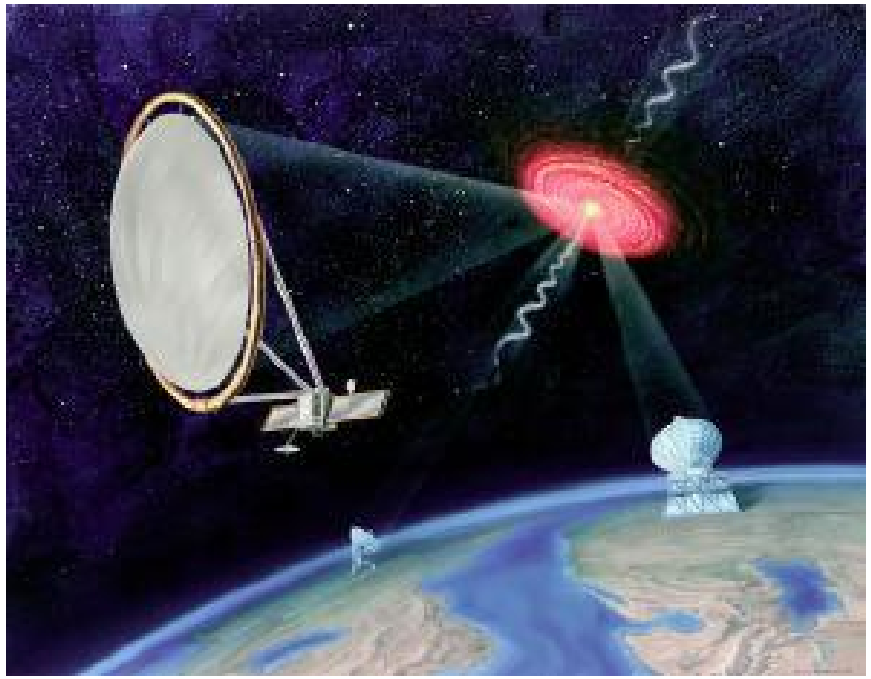

The 25m diameter ARISE Antenna Concept for VLBI (NASA JPL)
RIGIDIZABLE MATERIALS FOR USE IN GOSSAMER SPACE INFLATABLE STRUCTURES

High temperature and high performance polyimides which have a high glass transition temperature, withstanding a high temperature for a long period of time in air and in an inert atmosphere, and posses unusual stability. Harsh Space environmental conditions, including atomic oxygen resistance, ultraviolet and vacuum ultra resistance, low color/low solar absorption, electron and proton resistance, chemicals, moisture, electric fields, mechnaical stress, radiation and heat

Polyimides and their application

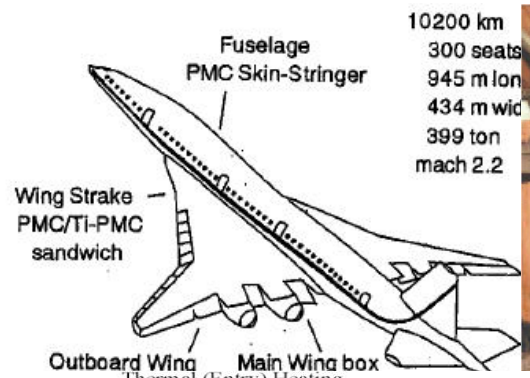

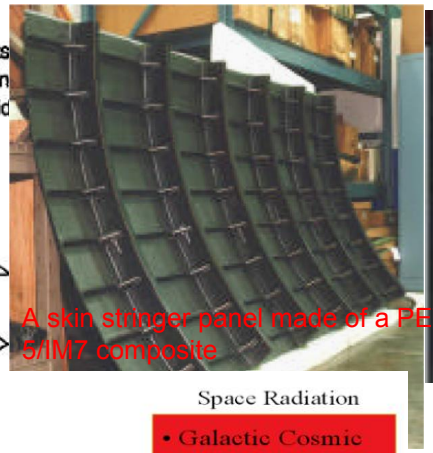

A skin stringer panel made of a PETI-5/IM7 composite

Thermal (Entry) Heating
Gas temperatures 15, 000 K

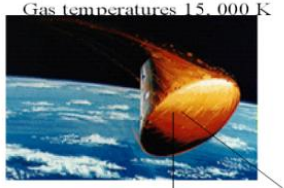

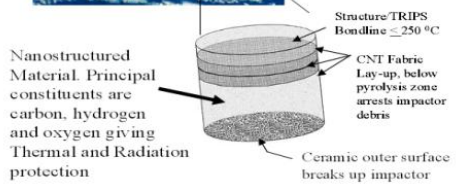

Space Radiation

- Galactic Cosmic Rays: e.g. Fe Ions, etc.
- Solar Flux
- Solar Flares

Orbital Debris
Micrometeorite
(MMOD) Impact

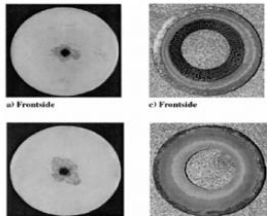

TRIPS: Systems analysis shows that Carbon Phenolic heat shield material for Apollo-style Lunar/Mars return can provide about 56 % of the suggested radiation shielding for a year’s exposure. TRIPS applicable to next generation outer planetary entry probes

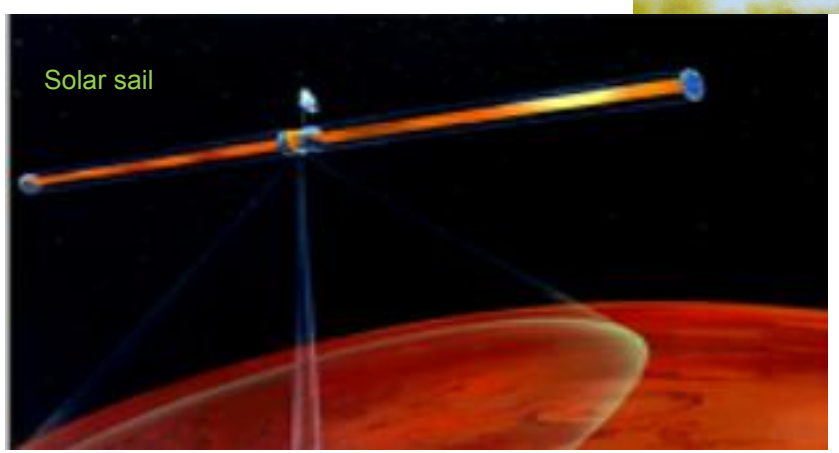

VENUS FLYER ROBOT
EXAMPLE MISSION PROFILE

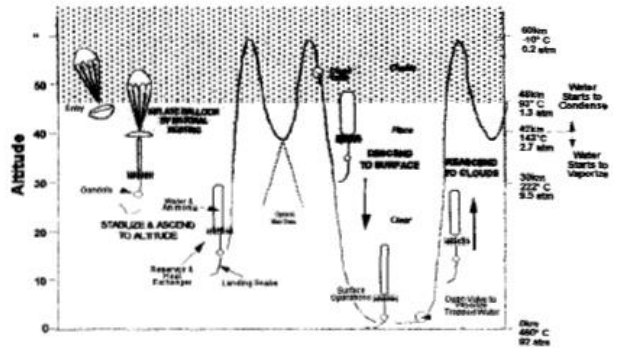

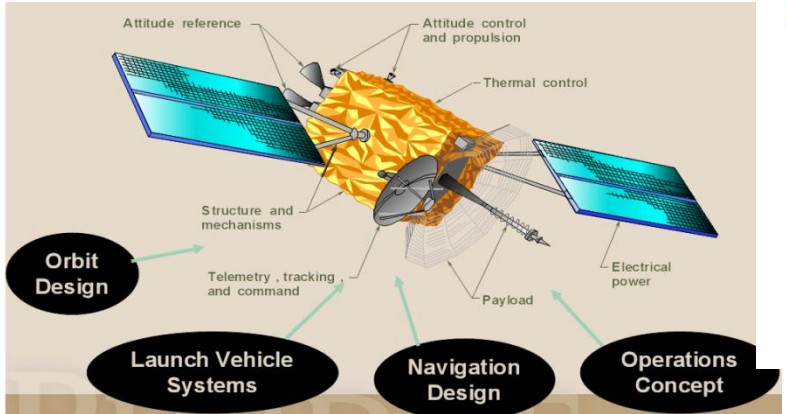

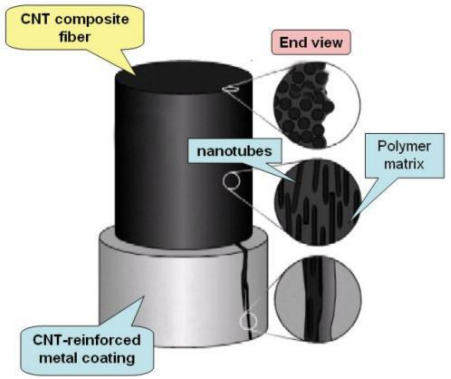

Application of CNT nanocomposites

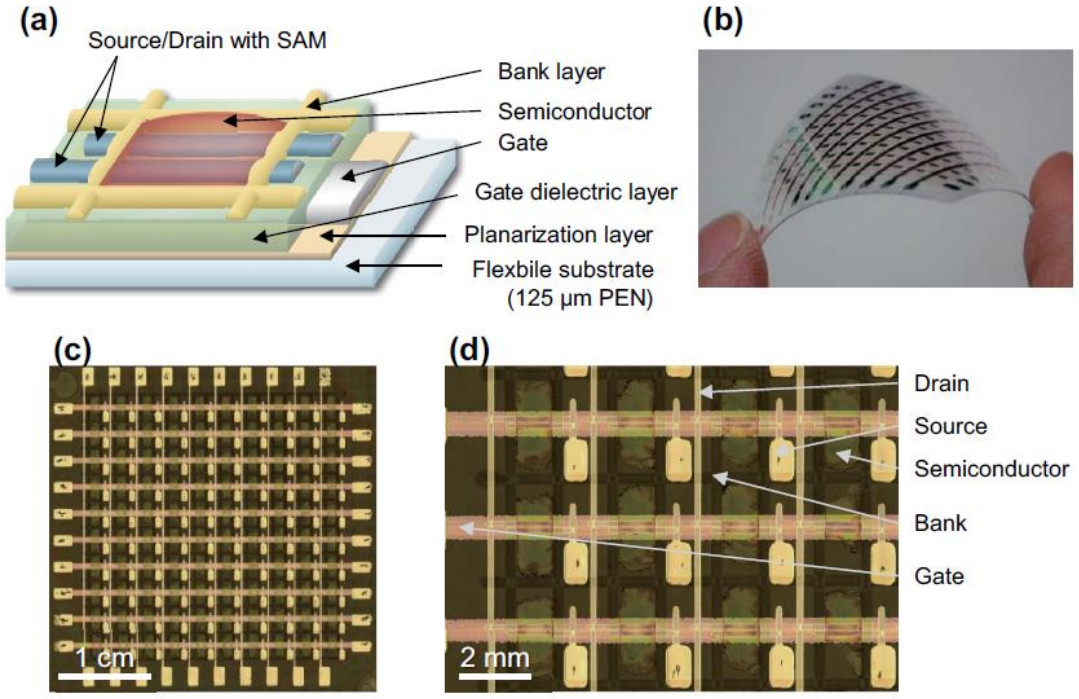

Fully solution-processed organic thin-film transistors on flexible substrates（https://doi.org/10.1038/srep03947）

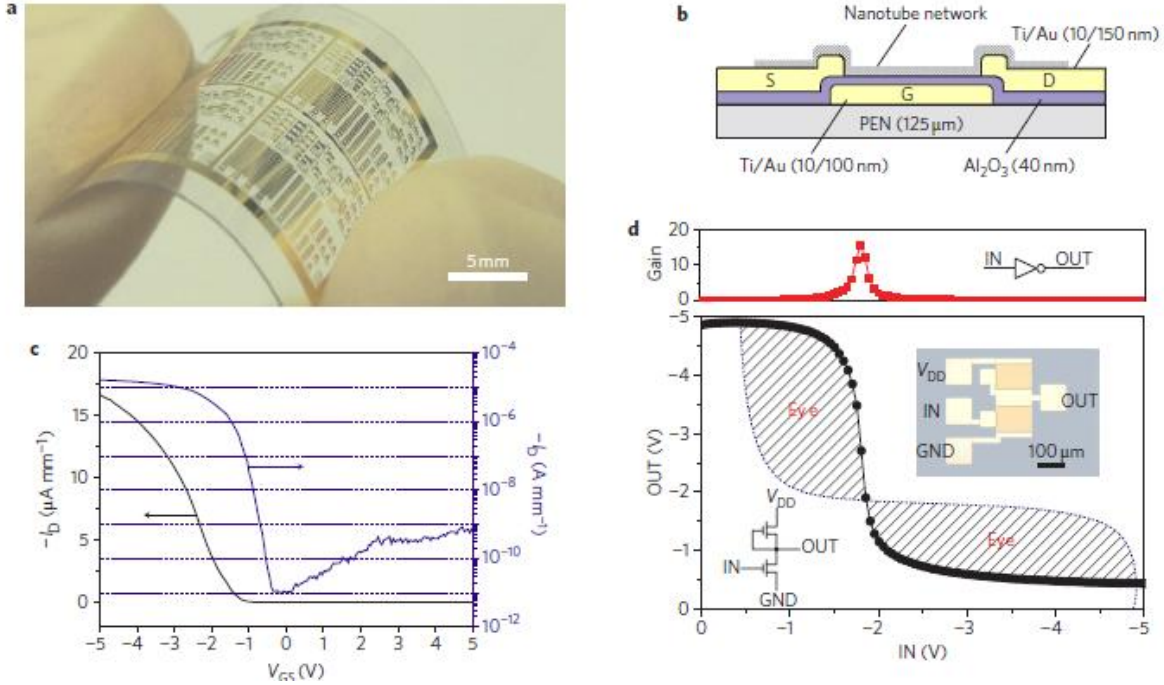

Carbon nanotube TFTs and integrated circuits on a flexible substrate（https://doi.org/10.1038/nnano.2011.1）

Induced dipole forces and London disperson force

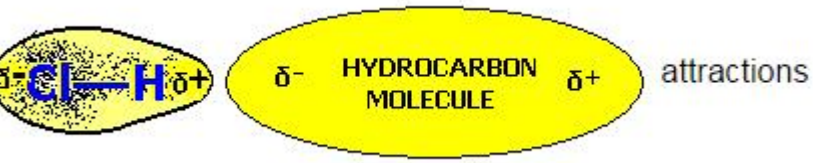

attractions

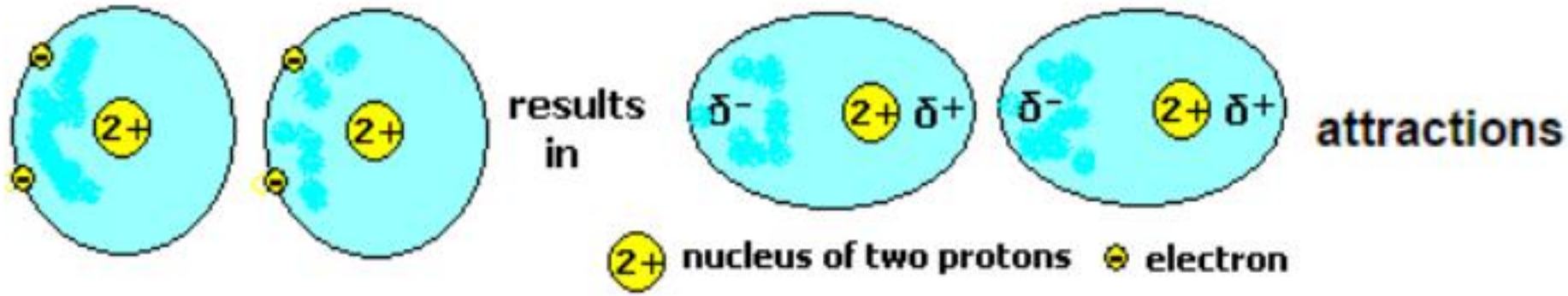

$$\frac{-m_1^2\alpha_2}{16\pi^2\varepsilon_0^2\varepsilon_r^2 r^6} = V$$

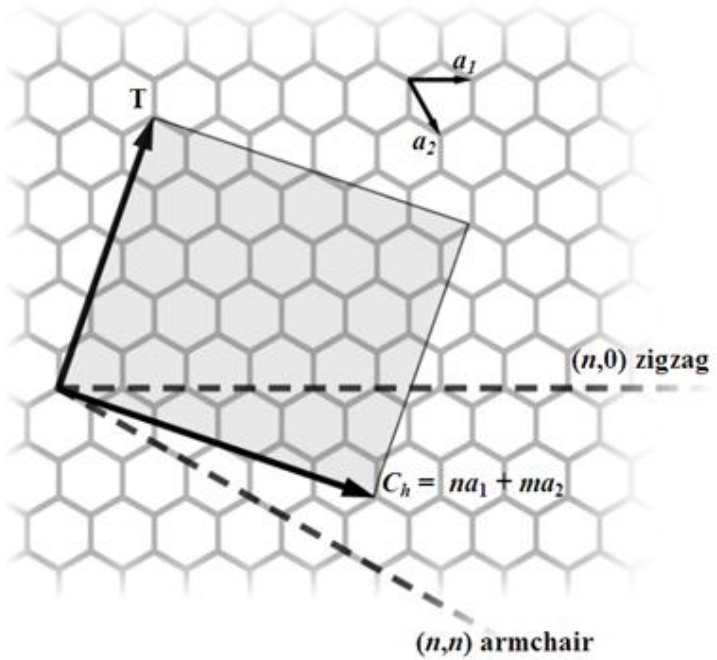

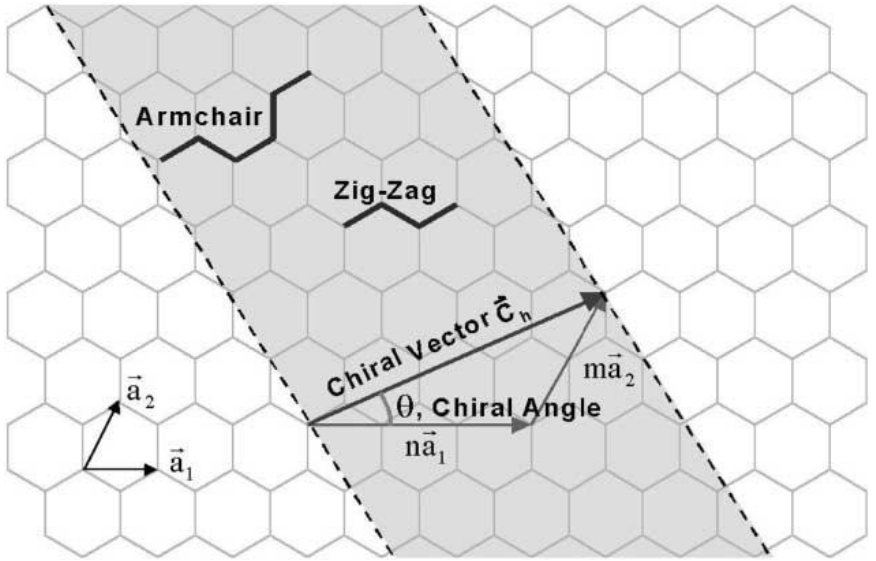

The (n,m) nanotube naming scheme can be thought of as a vector (Ch) in an infinite graphene sheet that describes how to "roll up" the graphene sheet to make the nanotube. T denotes the tube axis, and a1 and a2 are the unit vectors of graphene in real space

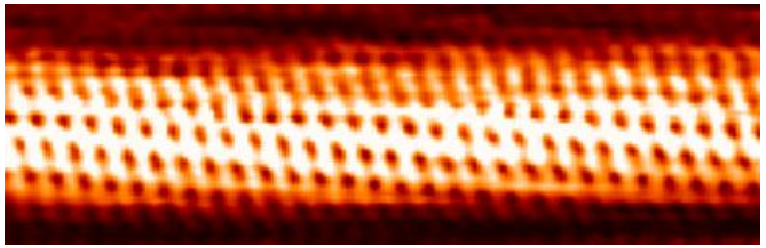

A scanning tunneling microscopy image of single-walled carbon nanotube

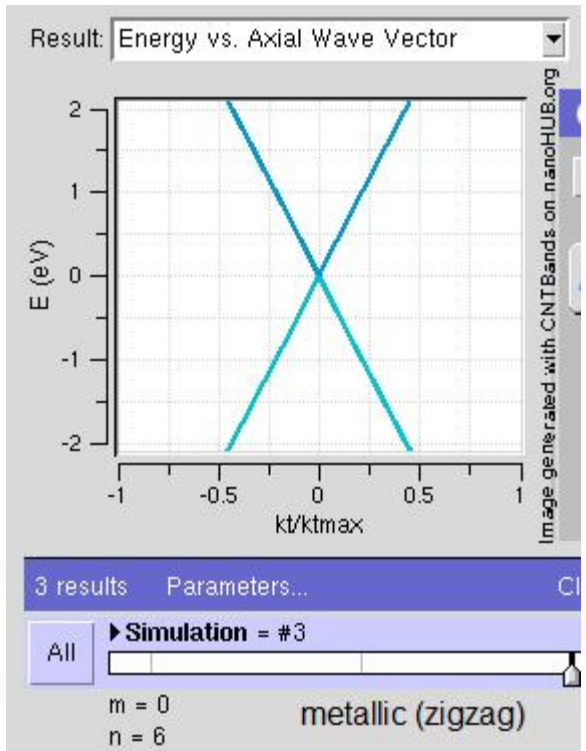
Result: Energy vs. Axial Wave Vector
E (eV)
kt/ktmax
Image generated with CNTBands on nanoHUB.org
3 results
Parameters...
All
Simulation = #3
m = 0
n = 6
metallic (zigzag)

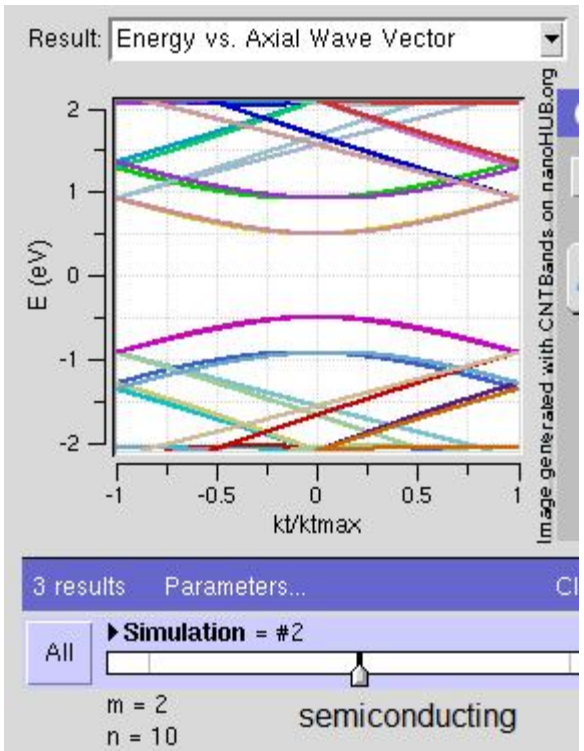
Result: Energy vs. Axial Wave Vector
E (eV)
kt/ktmax
Image generated with CNTBands on nanoHUB.org
3 results
Parameters...
All
Simulation = #2
m = 2
n = 10
semiconducting

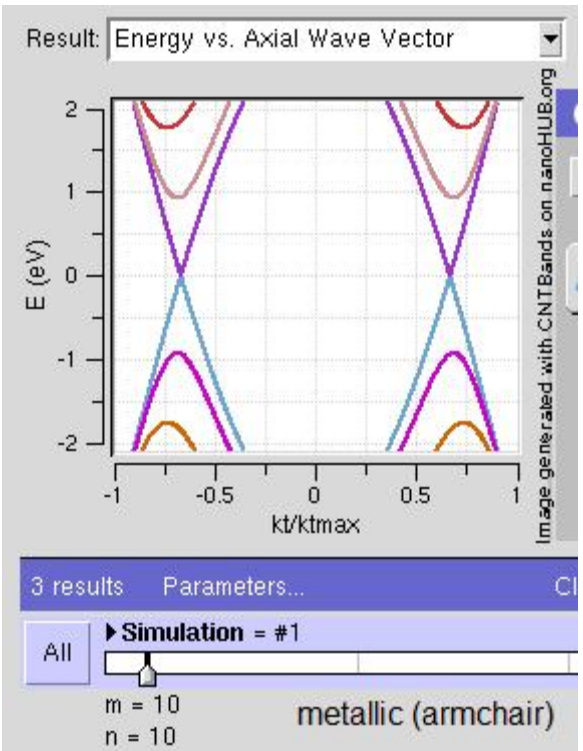
Result: Energy vs. Axial Wave Vector
E (eV)
kt/ktmax
Image generated with CNTBands on nanoHUB.org
3 results
Parameters...
All
Simulation = #1
m = 10
n = 10
metallic (armchair)

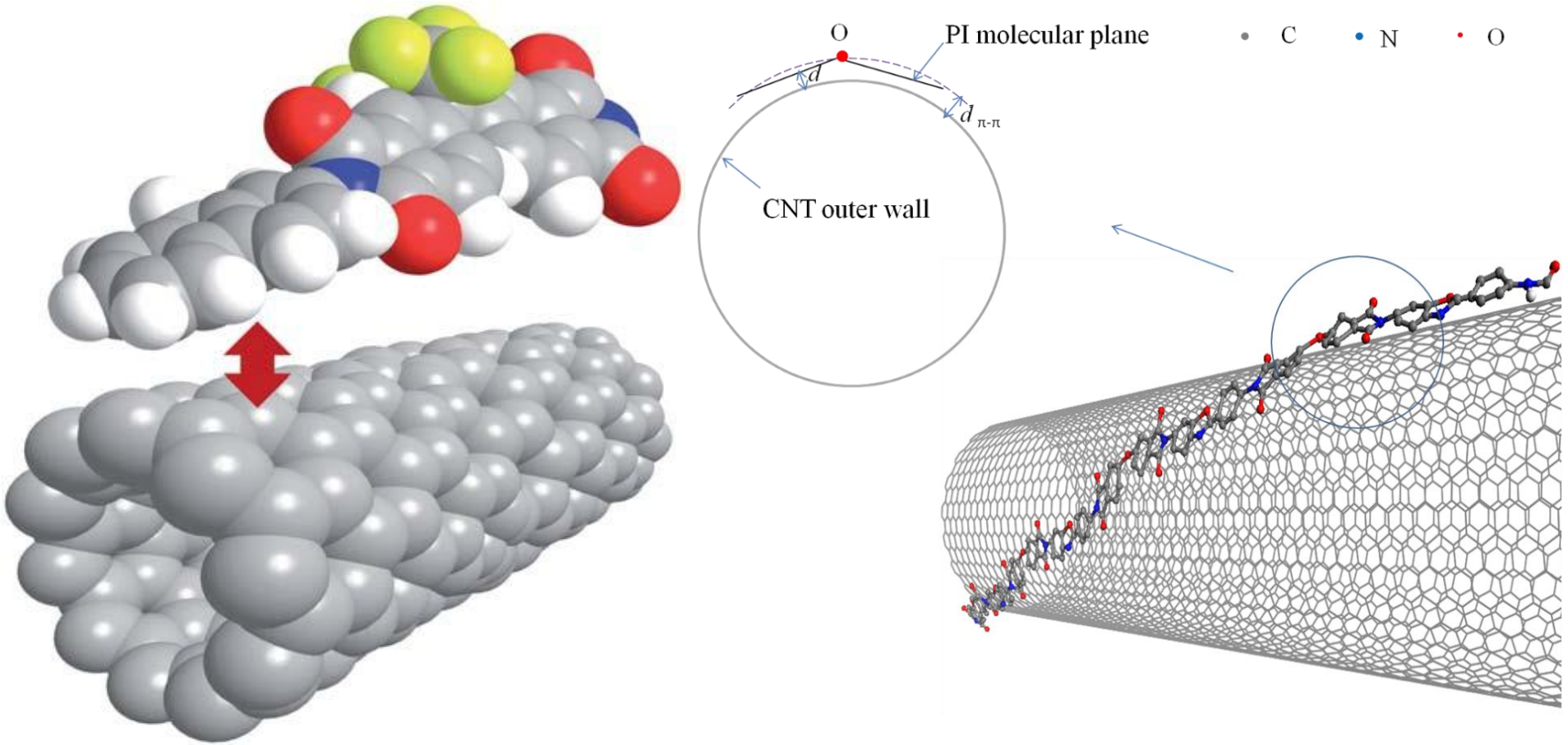

. Molecular interactions of polyimides with single-walled carbon nanotubesPolym. Chem., 2013, 4, 290–295

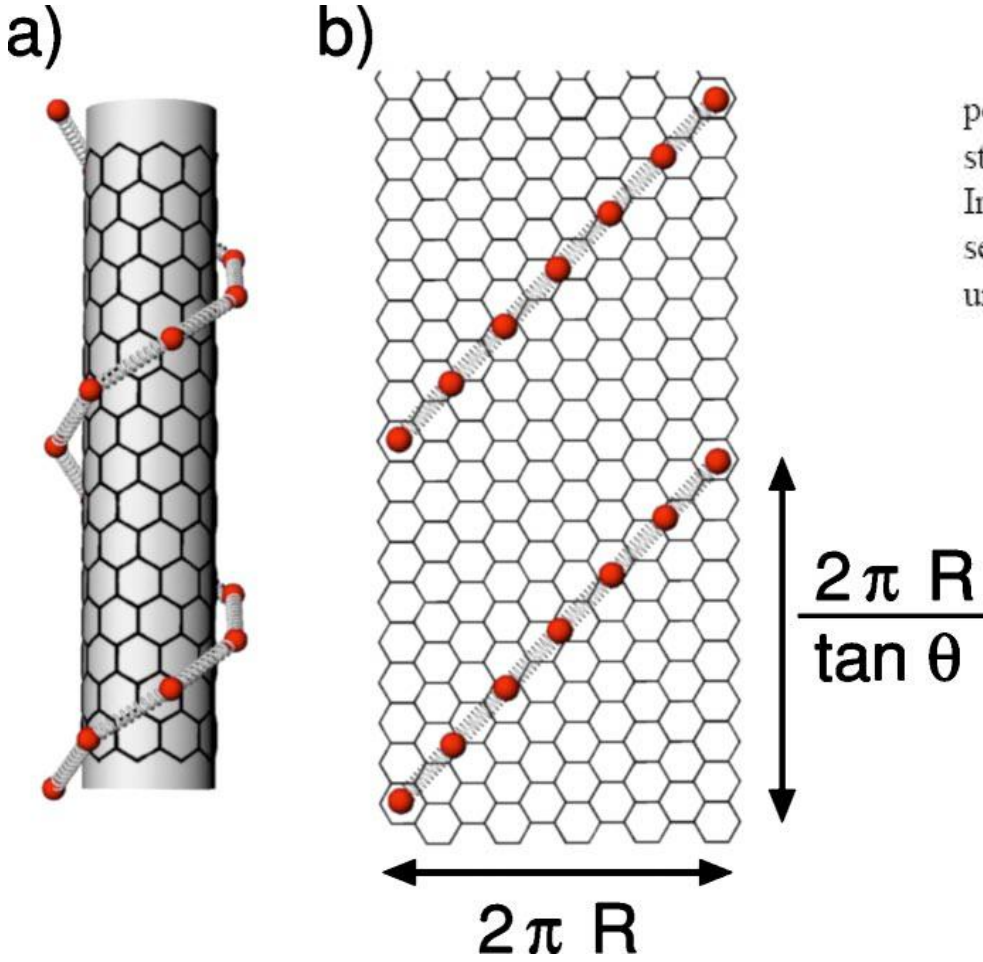

FIG. 1. (Color online) (a) Schematic representation of a single polymer strand coiling along the nanotube axis at an angle θ. The strand is represented by monomers connected by elastic springs. (b) In the two-dimensional depiction, the unwrapped tube is represented by a stripe of width $2\pi R$ and the coiling angle θ defines a unit cell of length $2\pi R/\tan\theta$.

The alignment process of polymer on CNT （Geometric constraints in the growth of nanotube-templated polymer monolayers ）

A. Wall, J. Coleman, M. Ferreira. Physical mechanism for the mechanical reinforcement in nanotube-polymer composite materials. Phys. Rev. B 2005, 71(12), 125421.

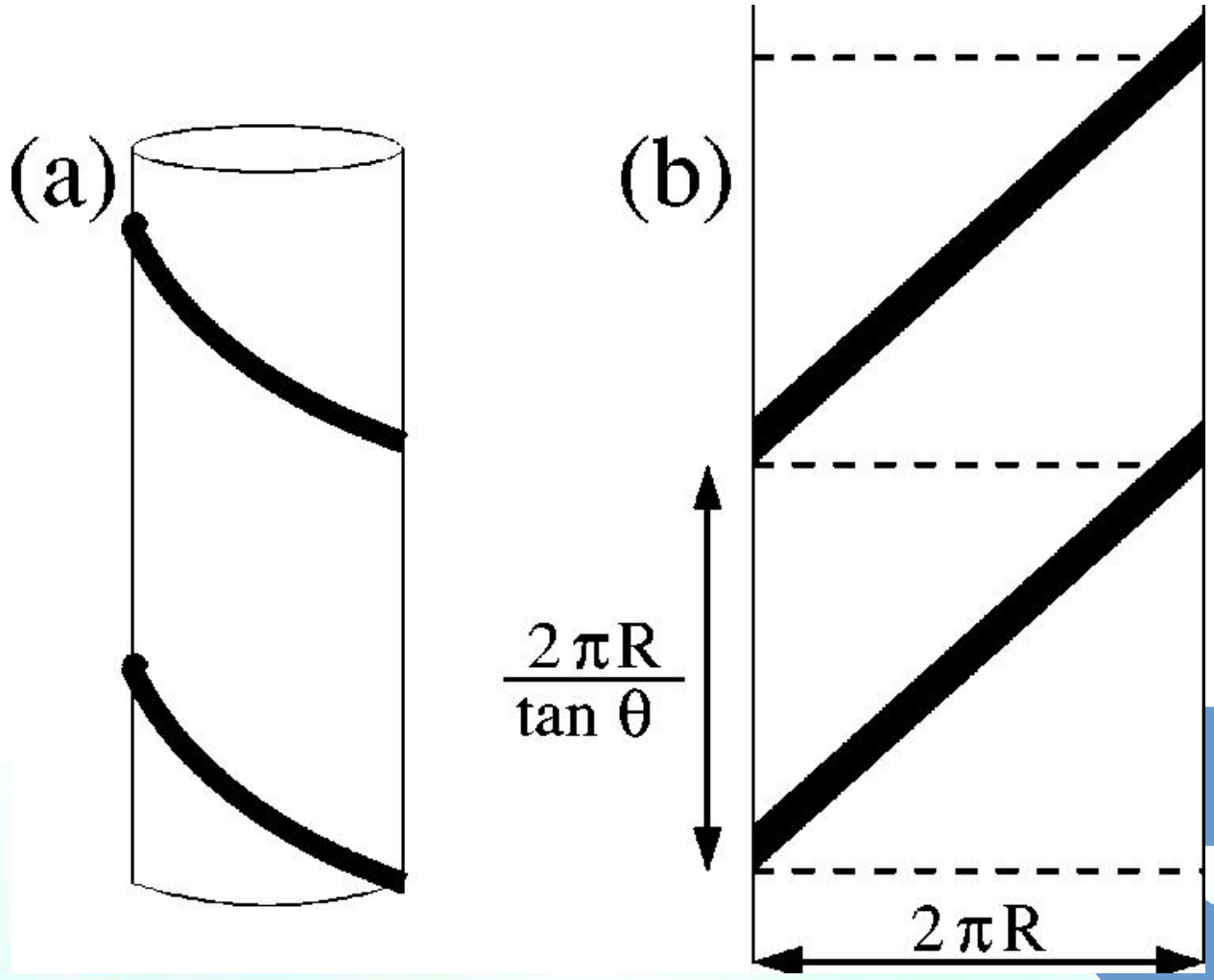

The van der Waals-based binding energy between the parts and the elastic-energy cost required to bend the polymer.

Appl. Phys. Lett., Vol. 84, No. 5, 2 February 2004

2 Experimental and methology

- In-situ polymerizaion of CNT/PI nanocomposites

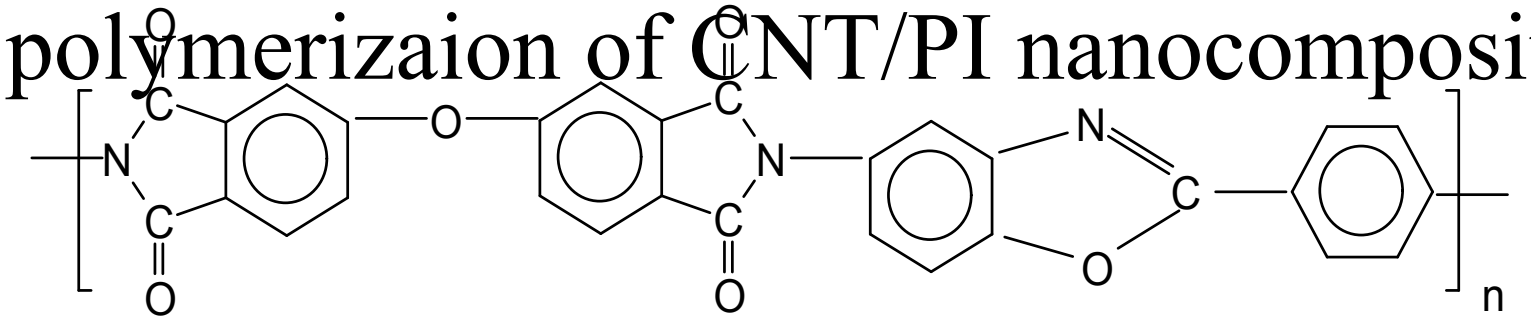

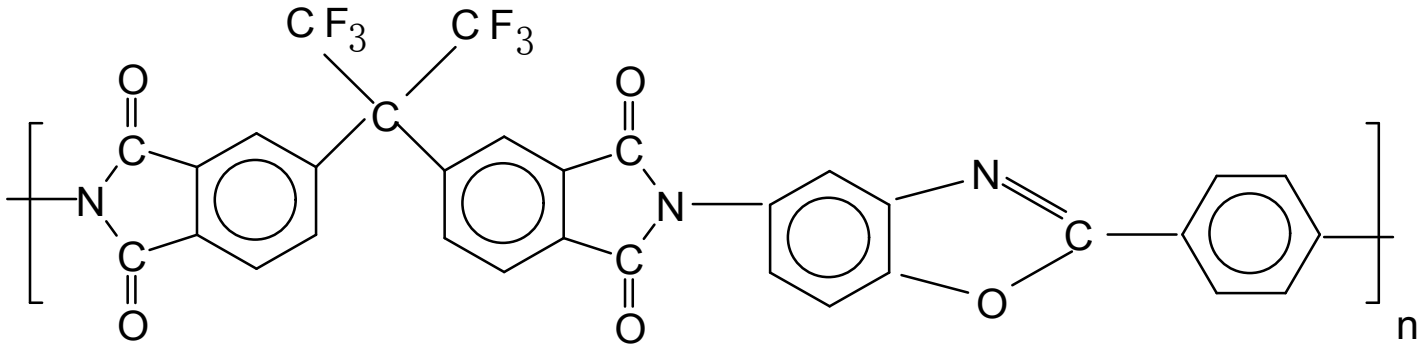

In-situ polymerizaion of CNT/PI nanocomposites

PI-I

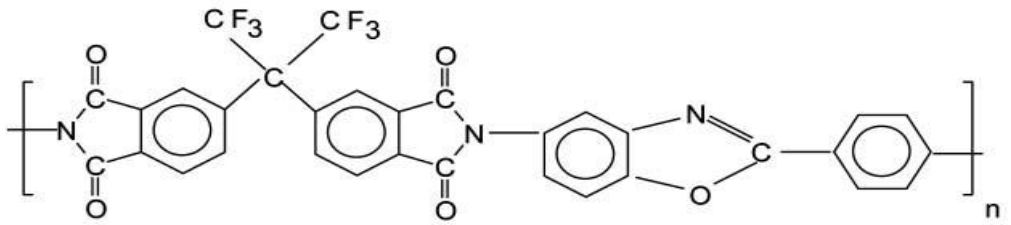

PI-II

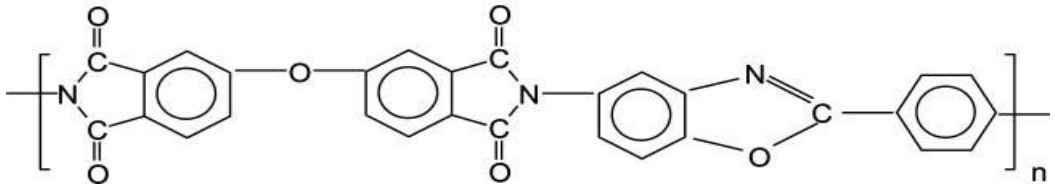

(a)

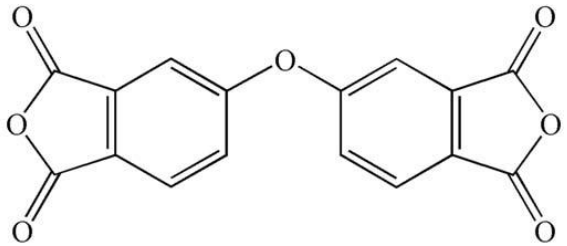

(a) ODPA

(b)

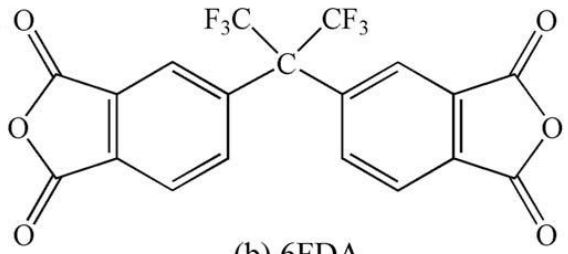

(b) 6FDA

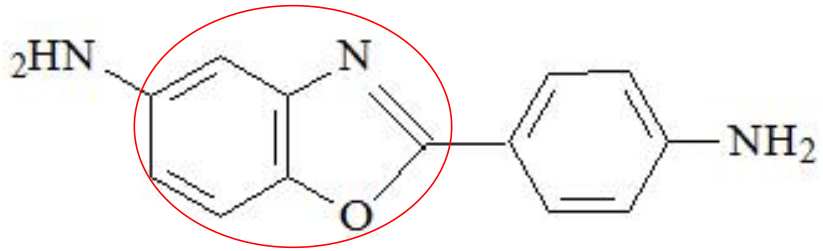

Rigid Benzoxazole ring improve the rigidity of the backbone of PI

Schematic illustration for in situ polymerization of CNT/PI(AAPB/ODPA) nanocomposites in the presence of COOH-CNTs

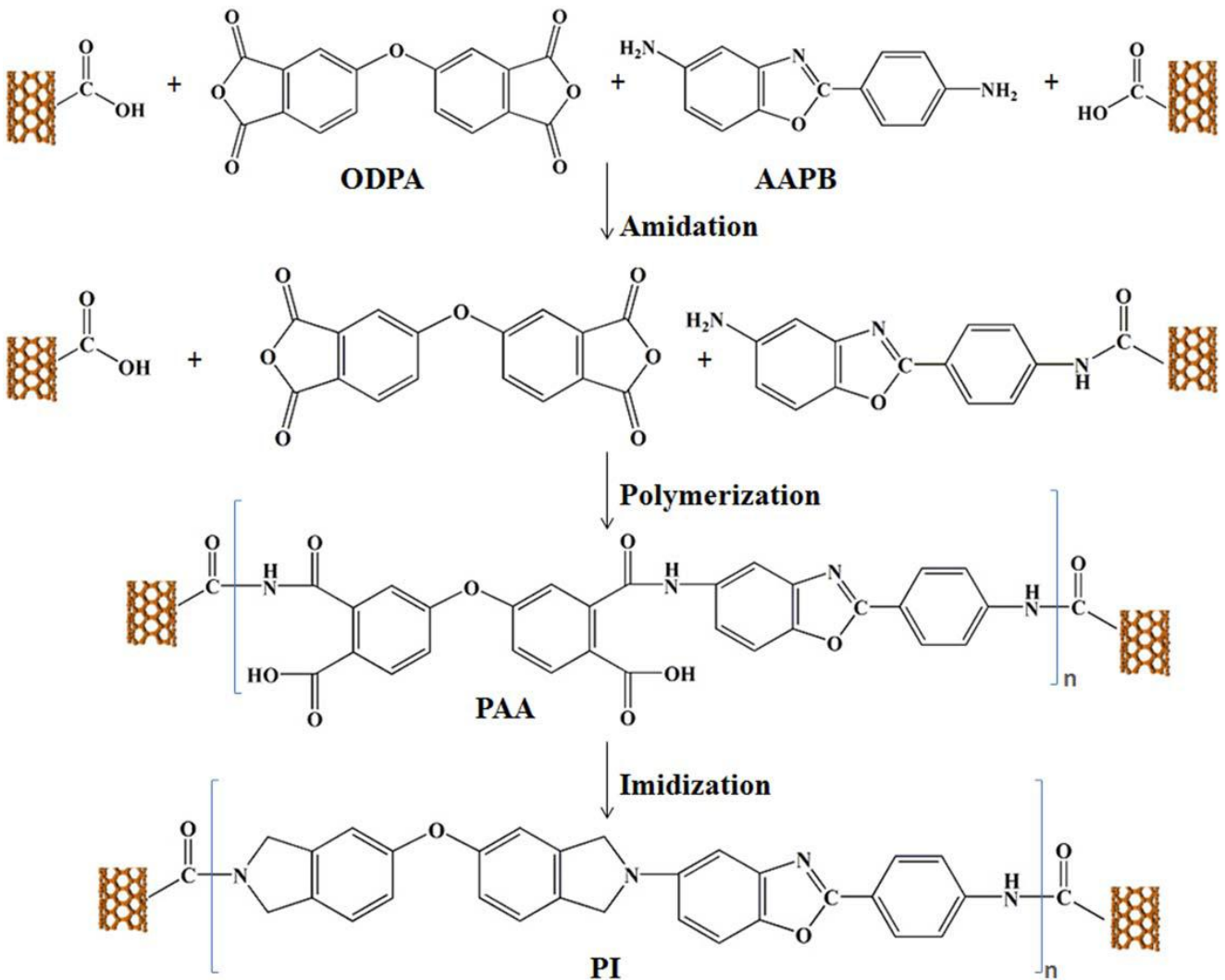

TEM image of CNT

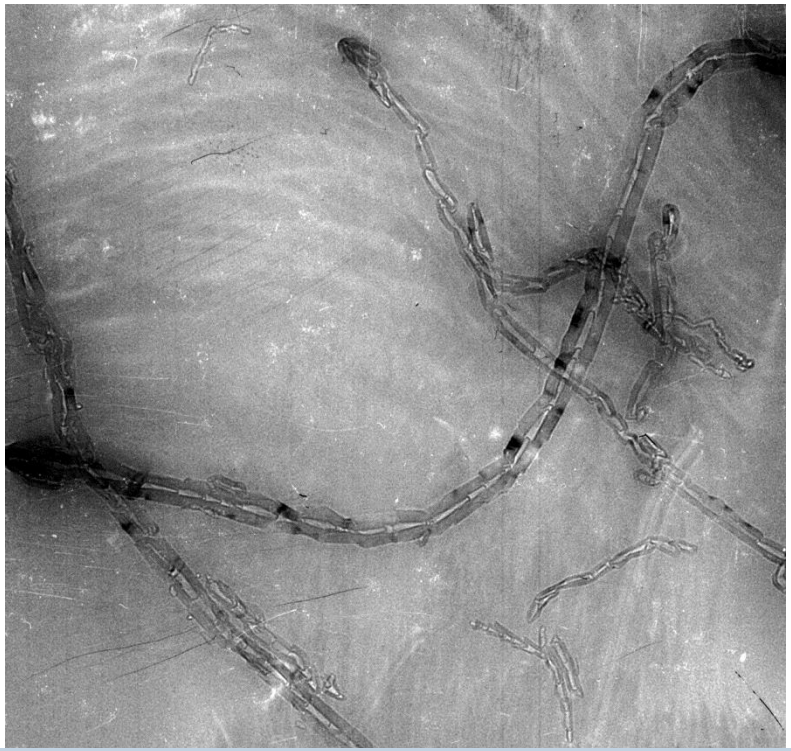

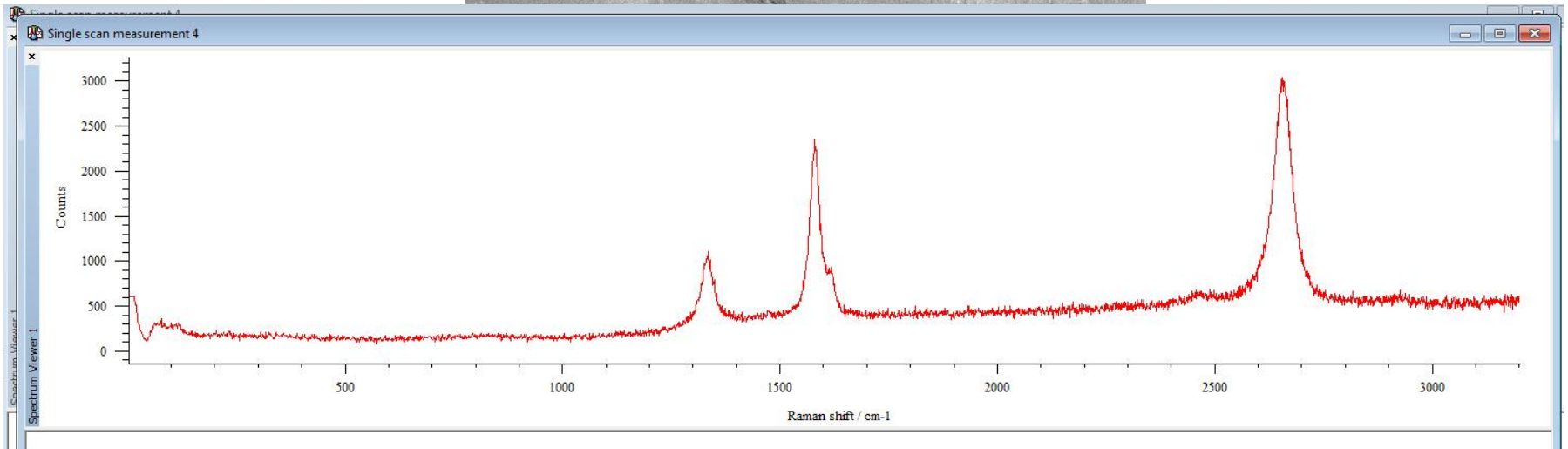

2.2 Methodology (computational method)

- 1 In order to qualitatively evaluate the dispersion energy deriving from phenyl moieties and benzoxazole ring, a symmetry-adapted perturbation theory (SAPT) analysis was employed. In an effort to understand the determinants of these interactions energy between aromatic PI and carbon nanotubes, we performed symmetry adapted perturbation theory (SAPT) calculations.
- 2 Armchair (222,222) type carbon nanotube (CNT) with diameter of 30.1 nm was chosen and its atomic coordinates were obtained using VMD Nanotube builder plugin. Using only a part of the nanotube surface for calculations was justified not only by computational cost, but also by the size ratio between nanotube and fragment/monomer.
- 3 Materials studio was employed to calculate the morphology of two PIs around CNT

R1

R2

R3

R4

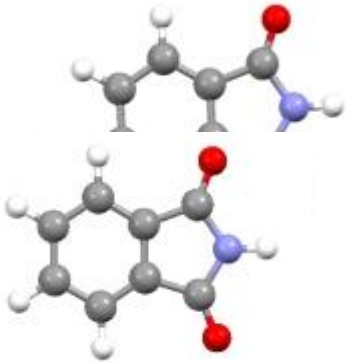

R5

Fragments R1-R5 after geometry optimization at B3LYP-D3/6-31G* level

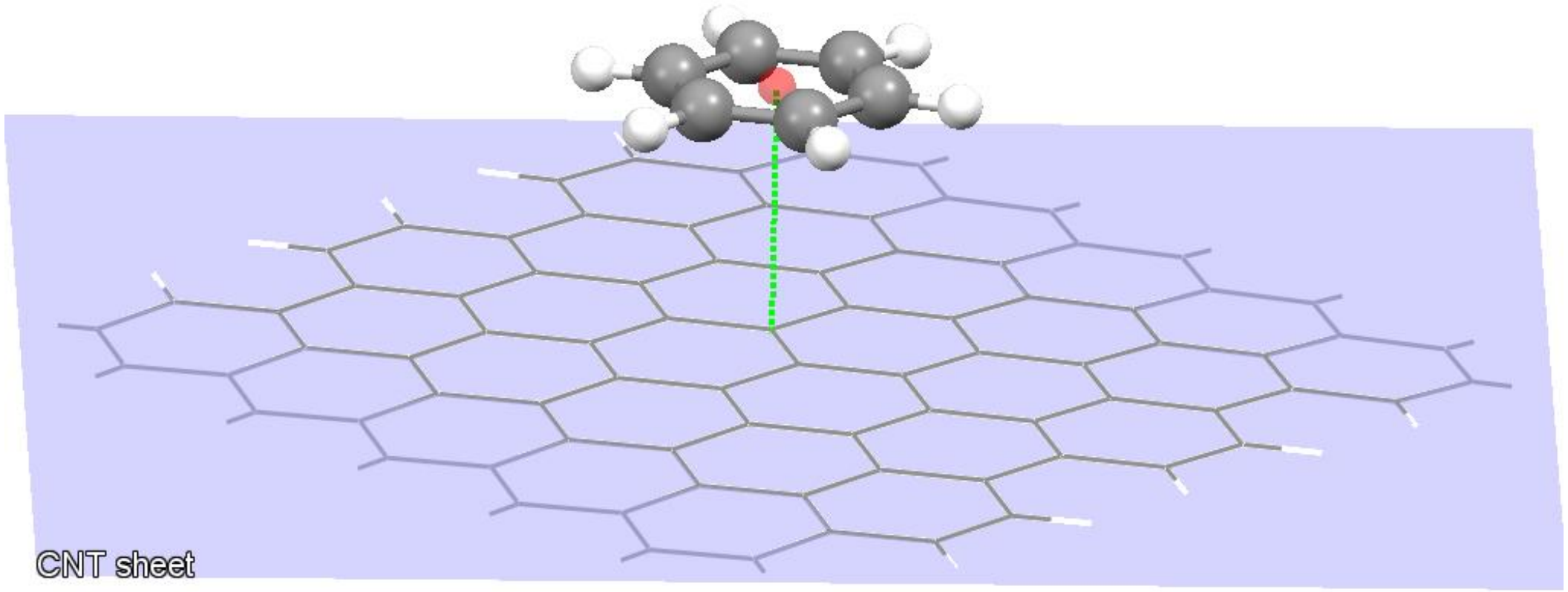

The R1 fragment parallel to smaller CNT sheet. The red sphere indicates the center of the six carbon atoms, the blue sheet is the plane of the CNT sheet, and the green dotted line is the normal distance (R) between the two. In case of fragments with conjugated ring systems, the center of the six-membered carbon ring was used to calculate the normal distance.

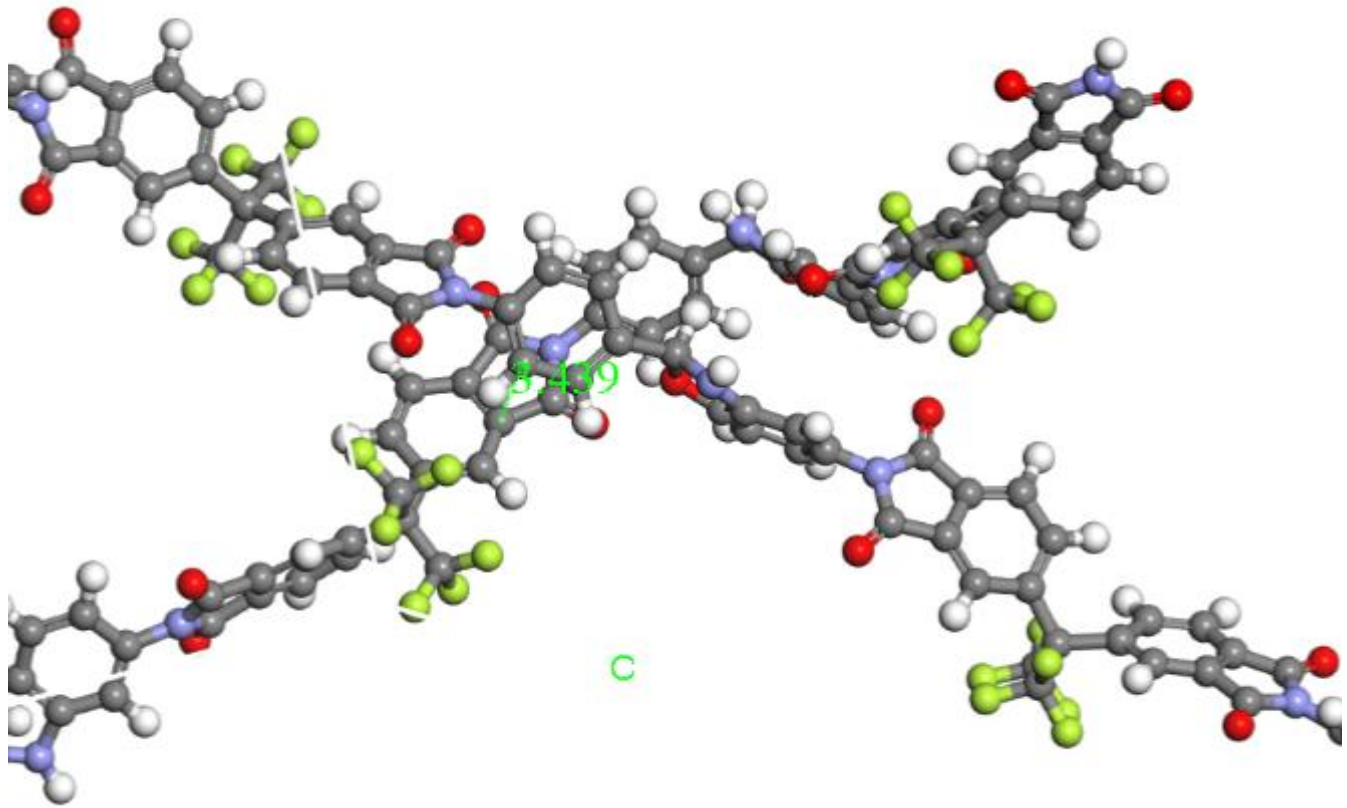
3.439
C

3 Results

- 3.1 Experimental results
- 3.2 Calculation results

3.1 Experimental results

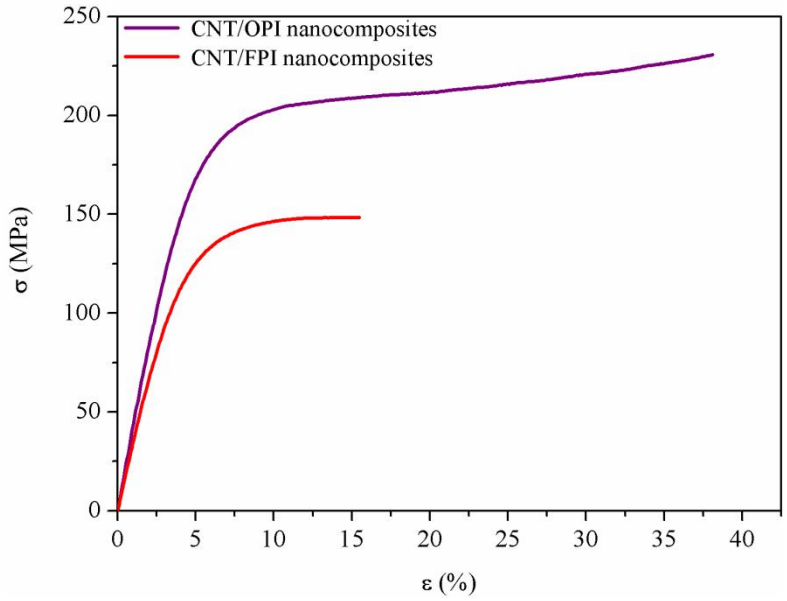

Figure The representative stress-strain curve of CNT/FPI and CNT/OPI nanocomposite films, respectively

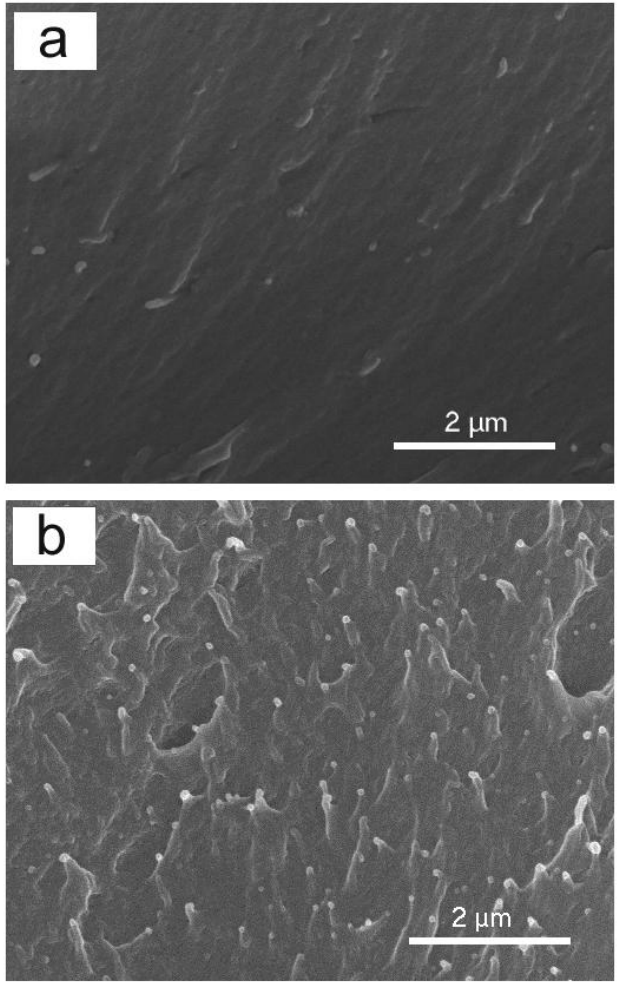

Figure 5 SEM of local fracture surface morphology of 0.5wt. %CNT/FPI (a) and 0.5% wt. CNT/OPI (b) nanocomposites

FT-IR, Raman and UV-vis Spectra of nanocomposites

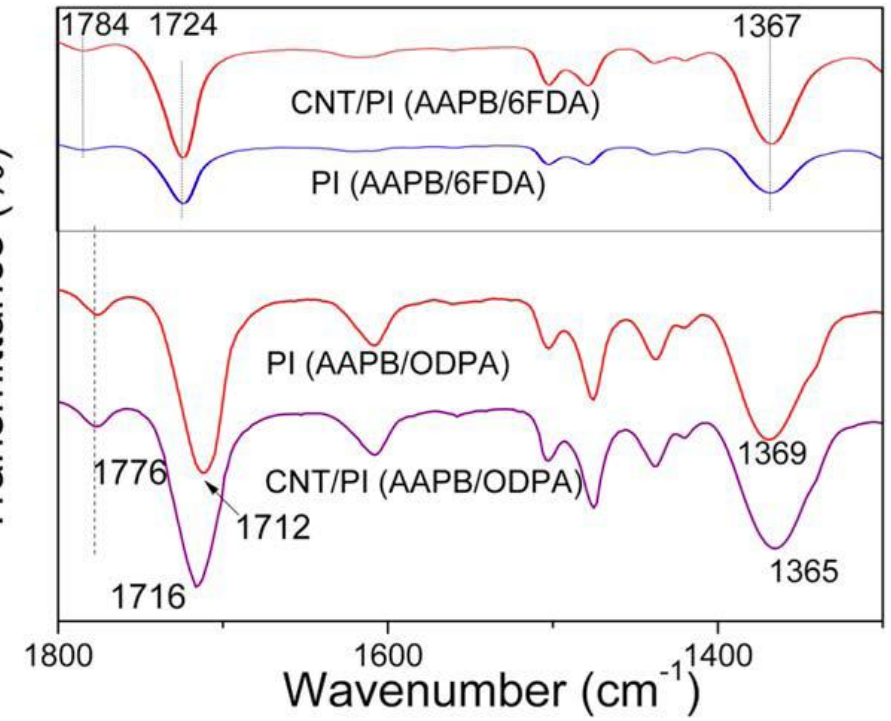

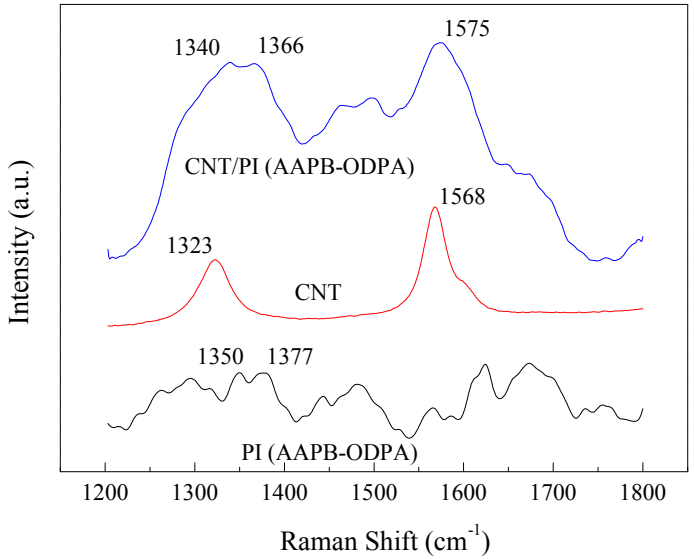

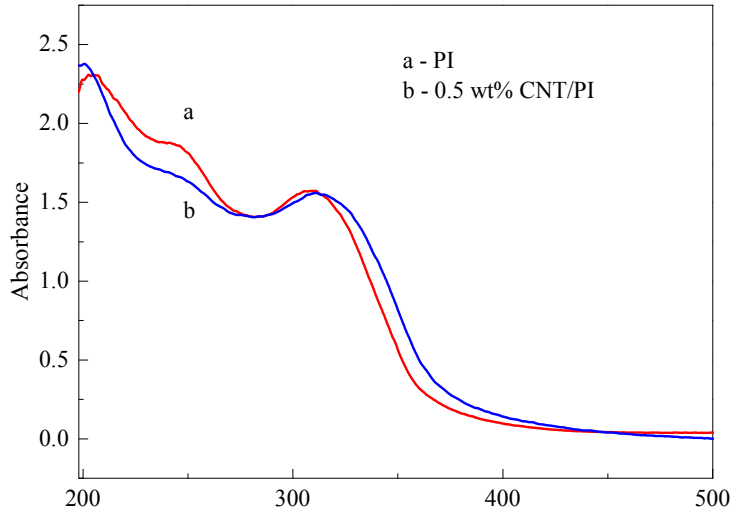

Amorphous PI and semi-crystalline PI and their nanocomposites

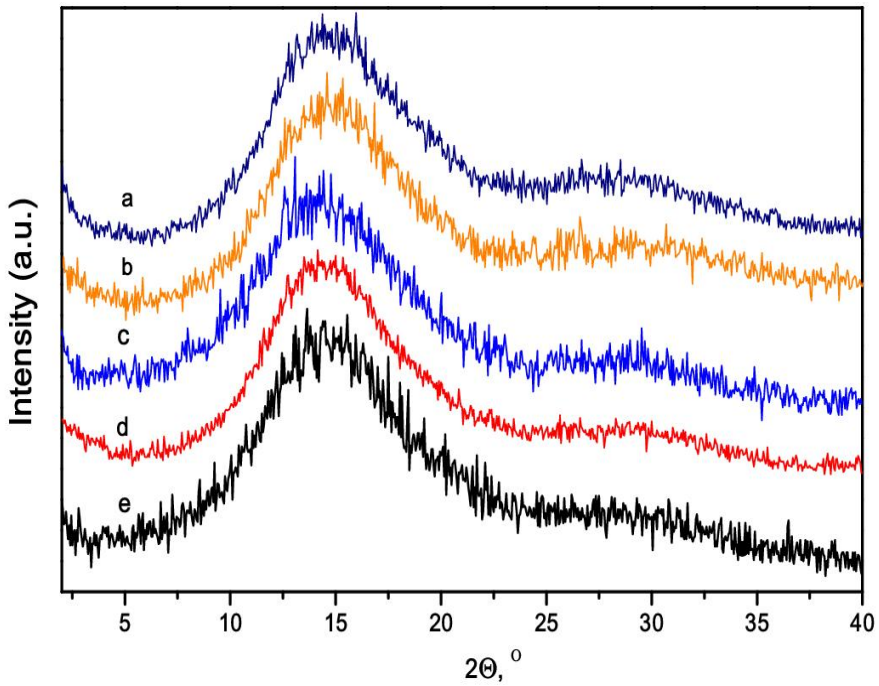

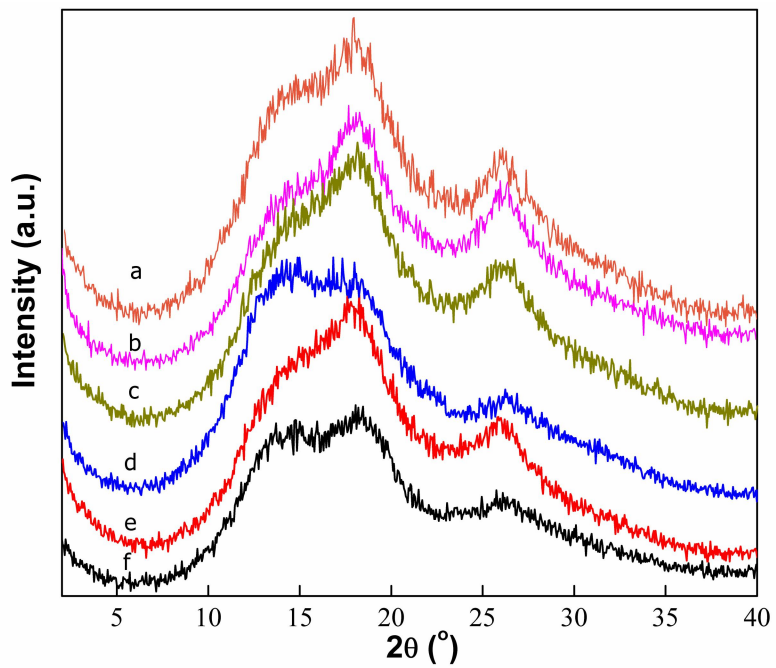

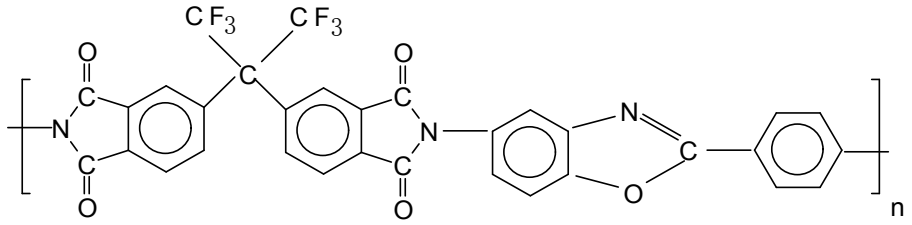

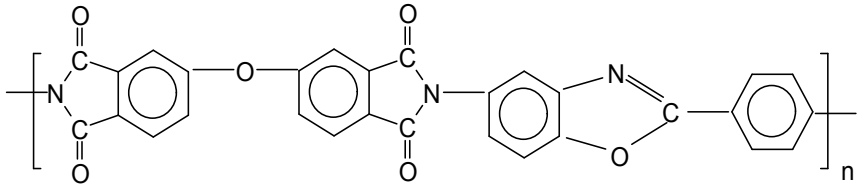

PL spectroscopy of CNT and two PIs

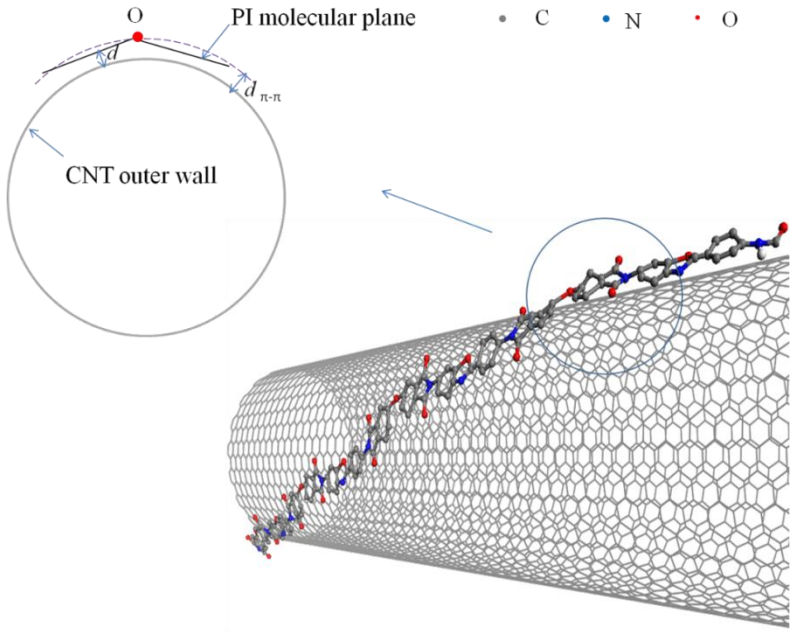

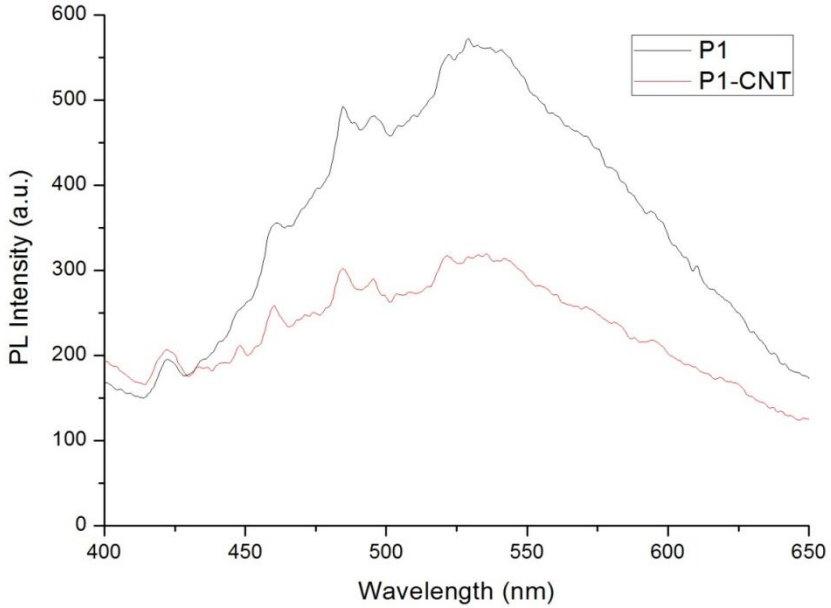

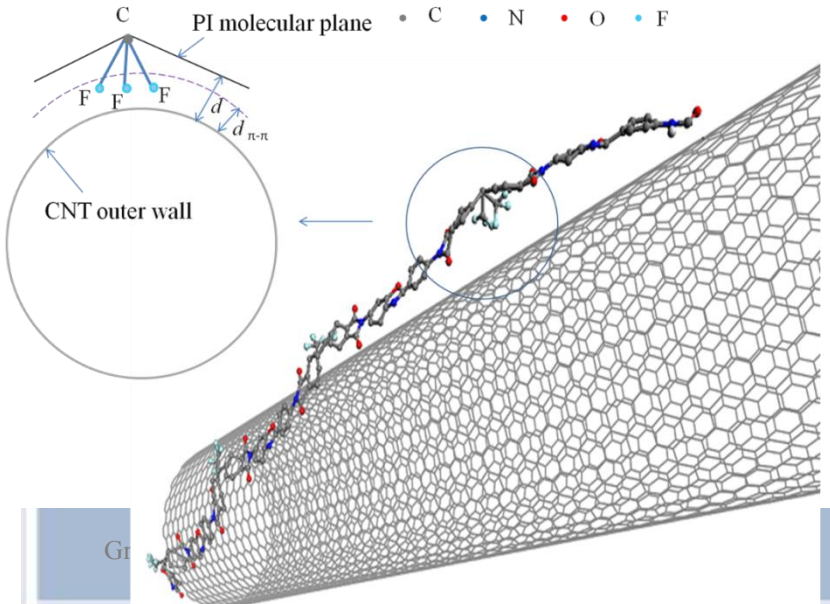

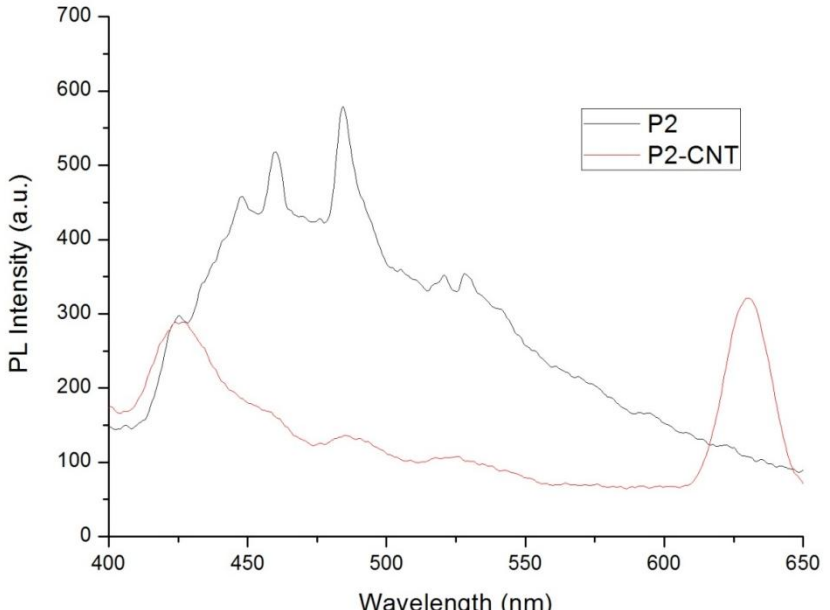

3.2 Calculation results

Table 1. The interaction energies (ΔE) and interaction energies per fragment electron ($\Delta E/n_e$) for fragment/CNT systems optimized at B3LYP-D3/6-31G* level.

	Normal distance R (Å)	ΔE (kcal/mol)	$\Delta E/n_e$(kcal/mol)
R1/CNT	3.383	-9.47	-0.2255
R2/CNT	3.318	-12.36	-0.1994
R3/CNT[1]	3.299	-16.99	-0.2023
R4/CNT	3.861	-16.13	-0.1090
R5/CNT[1]	3.376	-15.46	-0.2034

[1] the optimized geometry is in orientation III

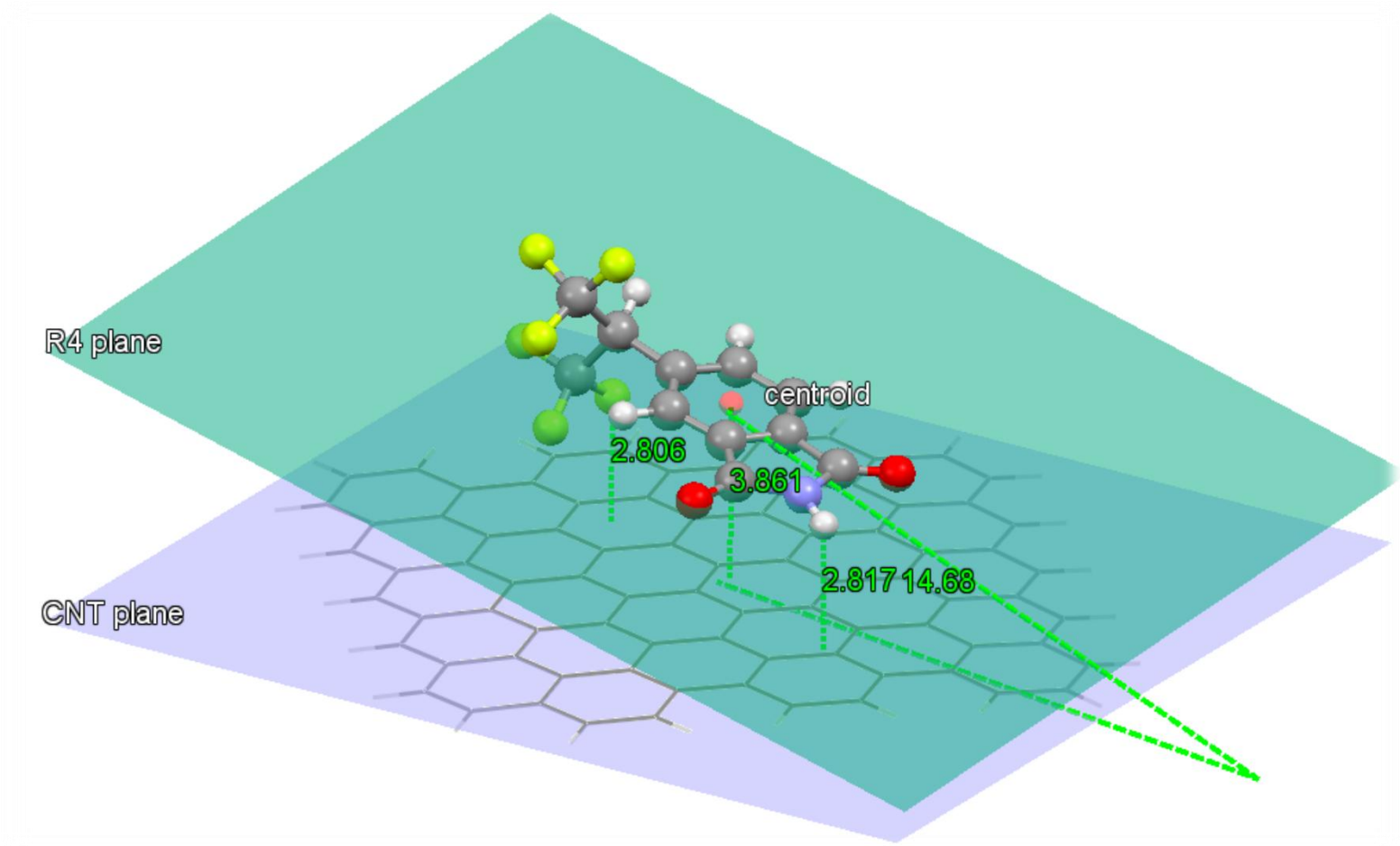

Figure 6. The geometry of R4/CNT system after full optimization at B3LYP-D3/6-31G* level starting from the geometry with fragment plane parallel to CNT sheet (Figure SI 2, orientation I). The figure shows relevant distances in the system and an angle between the CNT plane and the R4 plane after full geometry optimization.

Table 2. Normal distances (R), interaction energies (ΔE), and interaction energies per fragment electron ($\Delta E/n_e$) calculated at B3LYP-D3/6-31G* level for each fragment with CNT for coordinates obtained from energy minimization with GAFF force field.

	Normal distance R (Å)	ΔE (kcal/mol)	$\Delta E/n_e$(kcal/mol)
R1/CNT	3.405	-9.21	-0.2193
R2/CNT	3.464	-12.05	-0.1944
R3/CNT	3.406	-16.13	-0.1920
R4/CNT	3.978	-16.14	-0.1091
R5/CNT	3.406	-15.24	-0.2005

Table 3. Interaction energies (ΔE) and interaction energies per monomer electron ($\Delta E/n_e$) at B3LYP-D3/6-31G* level for two conformation of PI and FPI monomers with CNT in orientations obtained with MM energy minimization using GAFF force field.

Monomer/CNT	ΔE (kcal/mol)	$\Delta E/n_e$(kcal/mol)
0PI-1/CNT	-46.64	-0.1808
0PI-2/CNT	-45.84	-0.1777
FPI-1/CNT	-38.45	-0.1194
FPI-2/CNT	-39.13	-0.1215

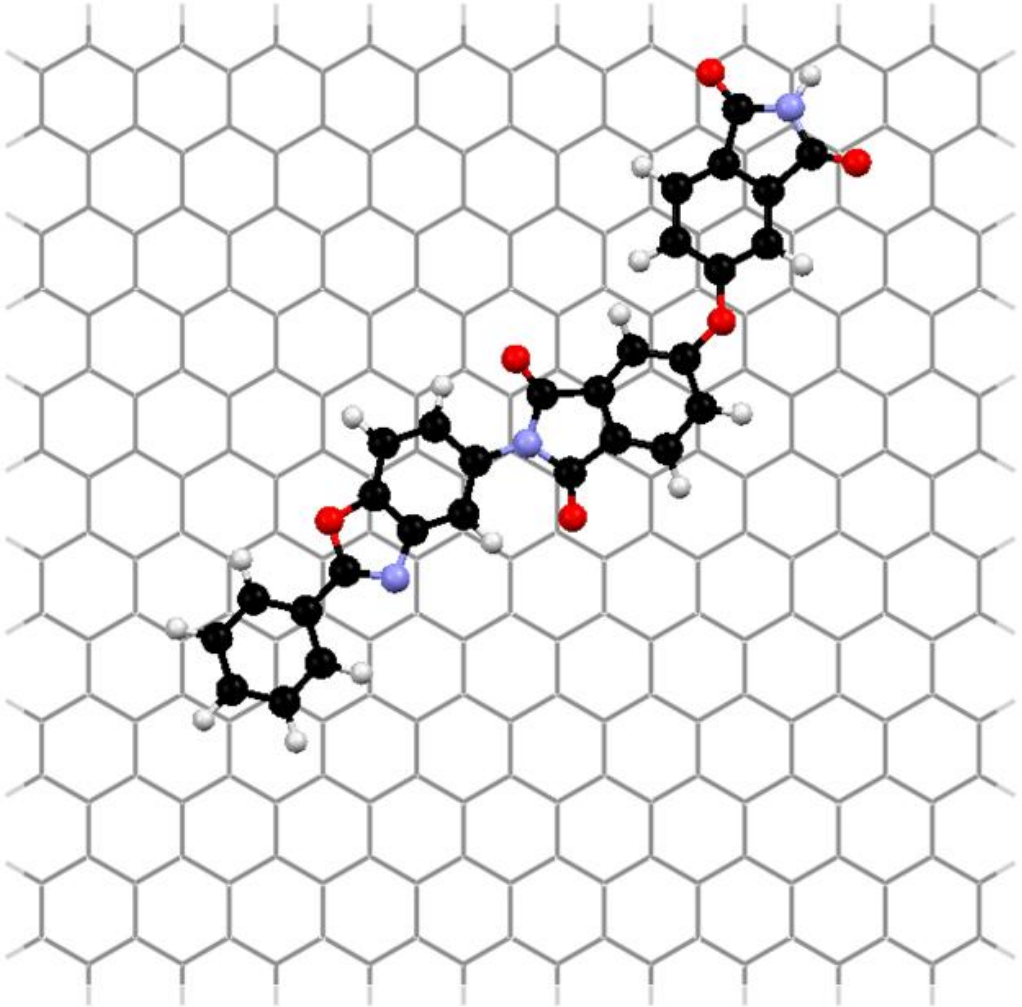

Figure 7. PI-1/CNT system after energy minimization with the GAFF force field. The interaction energy at B3LYP-D3/6-31G* level is -46.64 kcal/mol

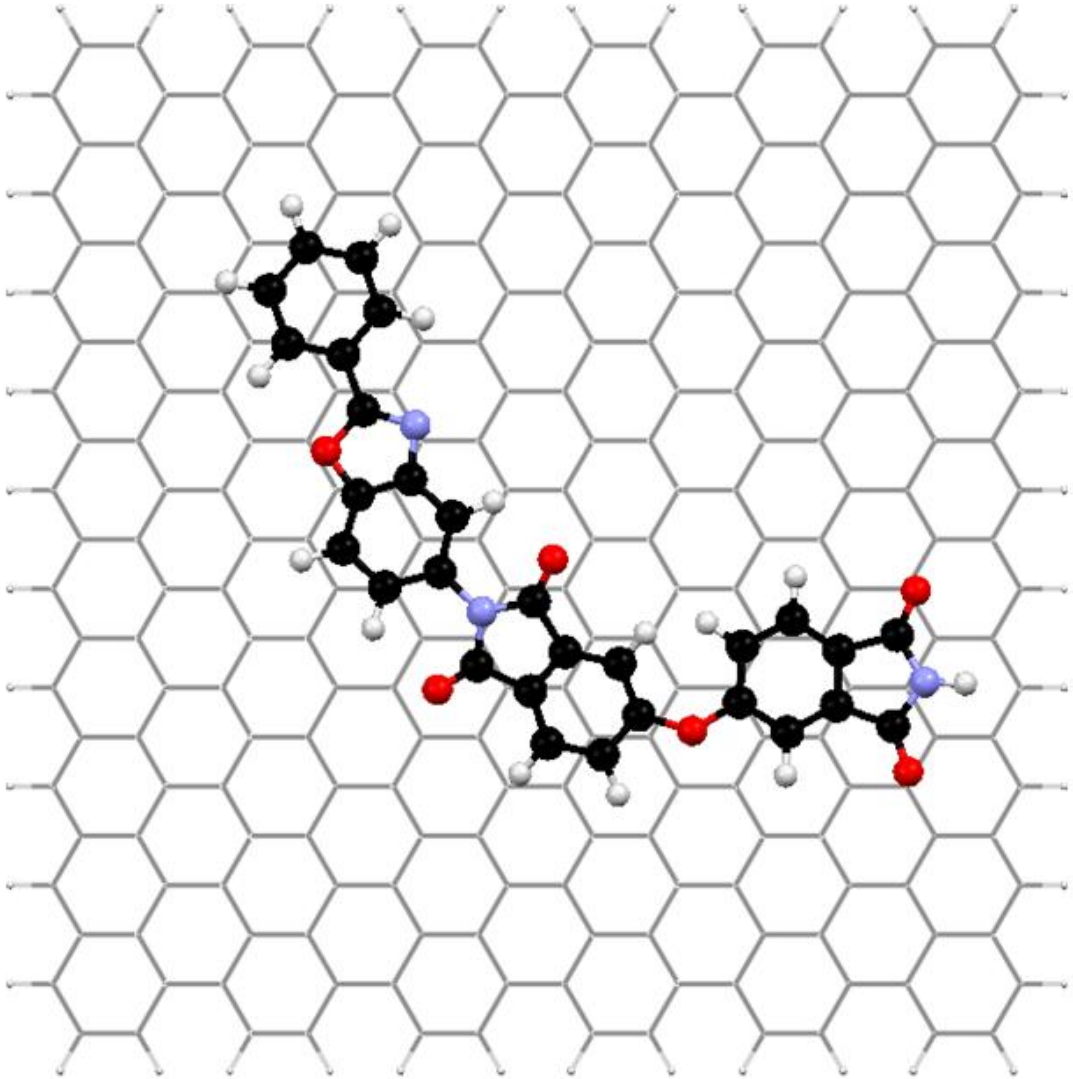

Figure 8. PI-2/CNT system after energy minimization with the GAFF force field. The interaction energy at B3LYP-D3/6-31G* level is -45.84 kcal/mol

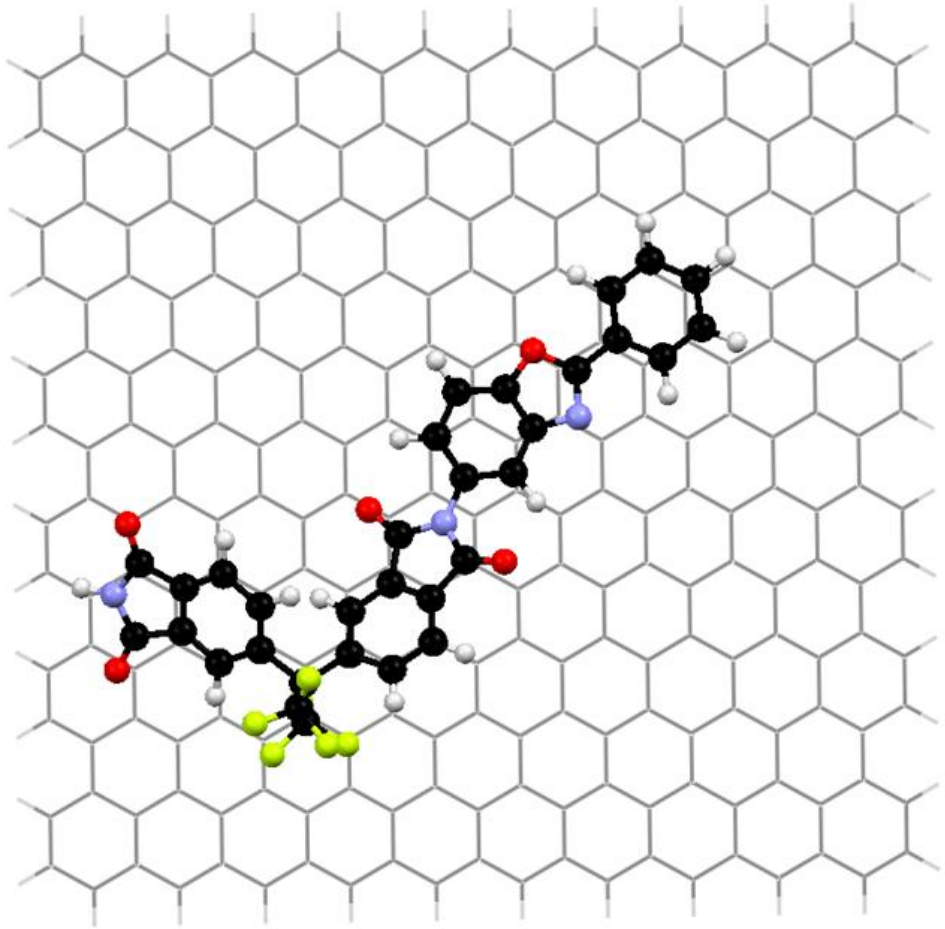

Figure 9. FPI-1/CNT system after energy minimization with the GAFF force field. The interaction energy at B3LYP-D3/6-31G* level is -38.45 kcal/mol

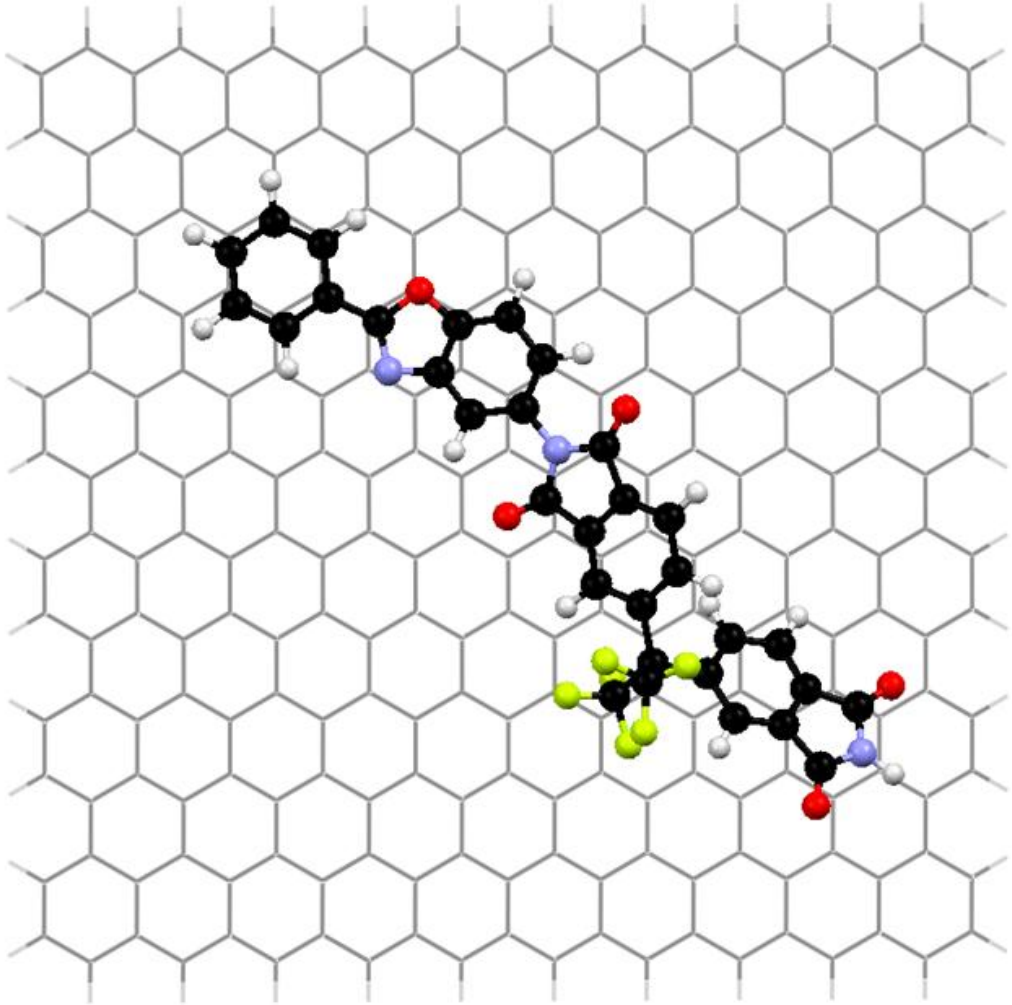

Figure 10. FPI-2/CNT system after energy minimization with the GAFF force field. The interaction energy at B3LYP-D3/6-31G* level is -39.13 kcal/mol

- Table 4. Decomposition of interaction energy at SAPT0/6-31G* level into electrostatic , exchange , induction and dispersion terms for each fragment with CNT sheet

		E_{el}	E_{ex}	E_{ind}	E_{disp}	E_{SAPT0}
R1/CNT	-5.62	+13.36	-1.08	-16.58	-9.93	
R2/CNT	-8.38	+20.02	-1.82	-24.60	-14.78	
R3/CNT	-11.32	+26.90	-2.92	-31.31	-18.65	
R4/CNT	-10.05	+26.29	-2.70	-30.17	-16.63	
R5/CNT	-10.14	+24.86	-2.73	-29.37	-17.37	

3 Materials studio calculation

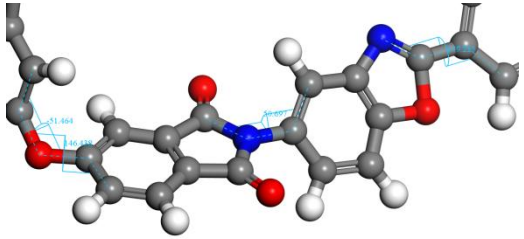

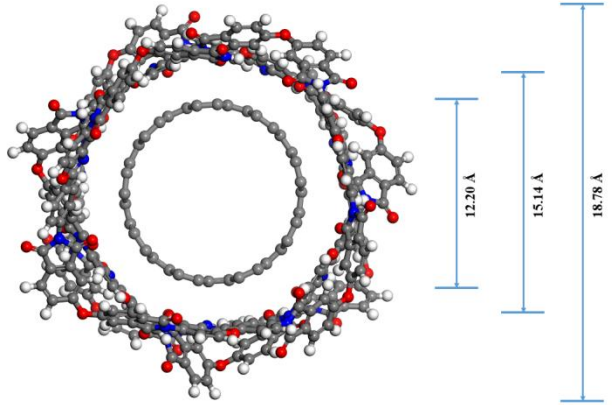

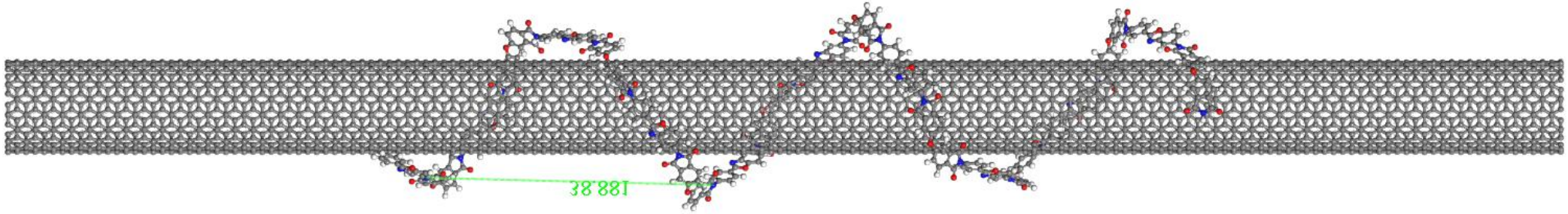

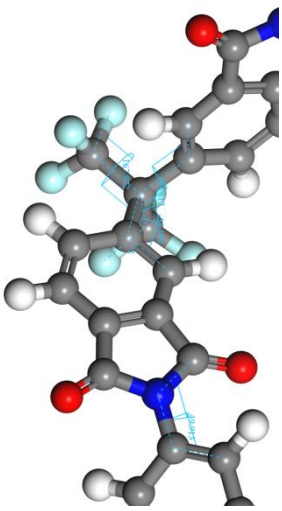

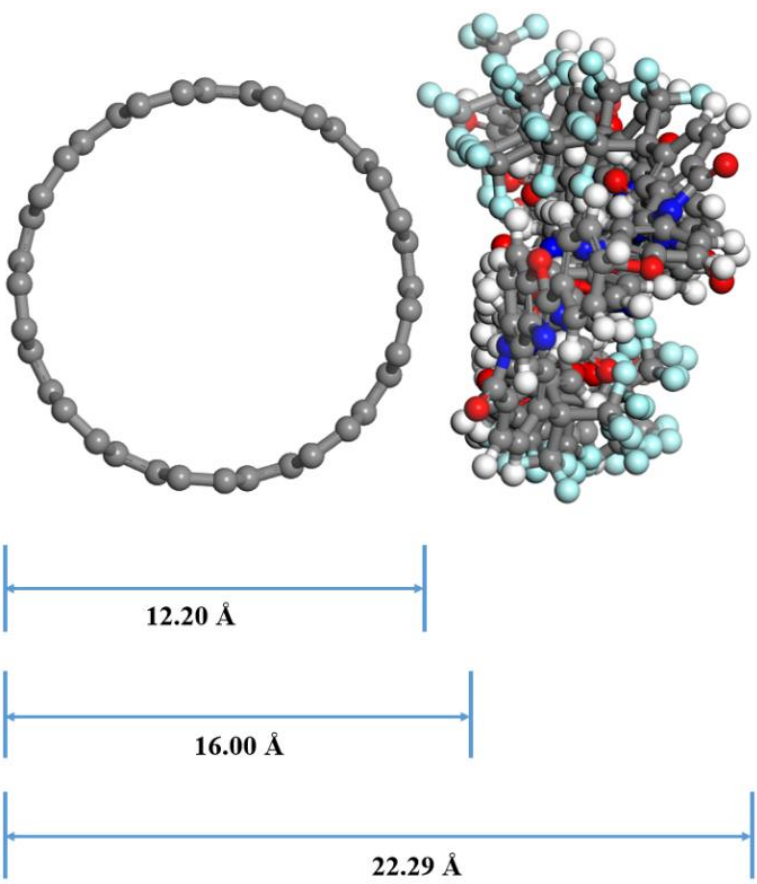
12.20 Å
16.00 Å
22.29 Å

4 Conclusion

- 1 Noncovalent interactions play an increasingly important role in nanocomposites in which nanoscale interactions between nanofiller and polymer matrix control composite interfaces. Monomer chemical structure play a crucial role in the interaction with CNT, the aromatic OPI with less steric effects adopt parallel confirmation to maximize the dispersion interaction with CNT, while the FPI with bulky group failed to take the parallel conformation around CNT.
- 2 The bulky 2(CF3)2 group inhibit the conformation due to steric strain. The CNT/FPI display a pull-out slip mechanism under uniaxial tension, the carbon nanotube was pull out of the surrounding polyimide chain, which indicates the weak interfacial interaction energy between CNT and molecule segments of FPI because of steric hindrance from nearby (CF3)2 change its conformation from a random from to more strained forms. The CNT/OPI nanocomposites display stronger interaction energy than that of FPI and shorter distance between monomer and carbon nanotube. In the case of PI with ether bond, it appears that is preferentially in the plane of the phenyl ring of the polyimide backbone.

- 3 in the process of the in-situ polymerization of polyimide in the presence of carbon nanotubes, the flexible polyimide molecules prefer to assembly actively around the rigid nanotubes driven by London dispersion. However, due to the Pauli repulsion arising from steric effects, the two polyimides with different substituent groups adopt different conformation around carbon nanotubes
- 4 OPI with ether bond substituent adopt parallel conformation with weak internal steric strain energy, which result in strong interaction energy between them. By contrast, the rigid nature of symmetry and bulky –C(CF3)2 groups of FPI, restrict parallel conformation, the FPI having to adopt tilting conformation with strong internal steric strain energy, which resulting weak interaction energy between them. The synergetic effect of conformation and interaction energy leads to different stress transfer efficient, and consequent different failure mode, CNT pull-out failure and CNT yielding failure.

Acknowledgement

- **Baltic-German University Liaison Office Project**

Baltisch-Deutsches HOCHSCHULKONTOR
BALTI-SAKSA KÕRGKOOLIDE BÜROO BALTIJAS–VĀCIJAS AUGSTSKOLU BIROJS BALTIJOS ŠALIŲ IR VOKIETIJOS AUKŠTŲJŲ MOKYKLŲ BIURAS

- **DAAD**

DAAD
Deutscher Akademischer Austauschdienst
German Academic Exchange Service